University of Alberta

Separation of Hydrogen and Carbon Dioxide from Syngas Using Clinoptilolite Natural Zeolite and Ordinary Portland Cement Composite Membranes

by

Omar Zarro

A thesis submitted to the Faculty of Graduate Studies and Research
in partial fulfillment of the requirements for the degree of

Master of Science

in

Chemical Engineering

Department of Chemical and Materials Engineering

©Omar Zarro
Spring 2014
Edmonton, Alberta

Abstract

Separating hydrogen and carbon dioxide from syngas is a necessary step for many industrial processes. Membrane separations are an attractive solution as they can operate at process temperatures (200-500 °C) and operate with a simple process.

Pure thermally stable (up to 600 °C) clinoptilolite zeolite was mixed with a Portland cement matrix, pressed, and cured to prepare composite membranes. Such systems offer scalable, thermally stable, and low cost membranes for H_2 and CO_2 separation from syngas.

Pure cement membranes demonstrated CO_2 impermeability. Single gas permeation measurement of H_2 and CO_2 was conducted and demonstrated high H_2/CO_2 selectivities up to 115 with permeances on the order of 10^{-9} mol/m^2·Pa·s for the composite membranes. The gas diffusion tests firmly exhibited molecular sieving toward H_2 and CO_2. These results suggest that cost-effective natural zeolites combined with ordinary Portland cement are capable of selective separation of H_2 and encourage future development of this concept.

Acknowledgments

First and foremost, I would like to thank my supervisor Professor Steven M. Kuznicki for giving me the opportunity to conduct this research as his student. I am grateful for his mentorship, encouragement, and patience.

I also would like to extend my thanks to the Helmholtz-Alberta Initiative and the Forschungszentrum Jülich's IEK-1 for allowing me the opportunity to conduct my experiments in their facilities for 8 months. It was a great experience in Germany; I made wonderful friends, and specifically I would like to thank Dr. Hans Peter Buchkremer, Dr. Matrin Bram, and Dr. Stefan Baumann.

I would like give special thanks to both Dr. James Sawada and Dr. Jan Hoffmann for their valuable support, encouragement, and friendship.

Many thanks go to all my colleagues throughout my studies; however, the following deserve much gratitude for their support: W. An, A. Zecko, B. Tanchuck, A.Shafie, P. Swenson, T. Kuznicki, W. Lan and A.R. Hejazi.

Finally, I would like to thank my parents and my brother for supporting me throughout my studies.

Table of Contents

List of Tables

List of Figures

Nomenclature

ALT   Air Leakage Testing

CSLM   Confocal Scanning Laser Microscopy

EDS   Energy-dispersive X-ray spectroscopy

GPM   Gas Permeation Measurement

IUPAC   International Union of Pure and Applied Chemistry

MFM   Mass flow meter

MMM   Mixed-matrix Membrane

PSA   Pressure Swing Adsorption

SEM   Scanning Electron Microscopy

STP   Standard Temperature and Pressure

Wt%   Weight Percent

XRD   X-ray Diffraction

α_{ij} The ideal selectivity for gas "i" over gas "j"

D_i Permeate diffusion coefficient for component "i"

j_i Volume (molar) flux for gas component "i" at STP, [cm^3/cm^2·s]

K_i Sorption coefficient for gas component "i" at STP,[cm^3/cm^3]

l Membrane thickness [mm]

M_i The molecular weight of gas "i", [mol/g]

M_j The molecular weight of gas "j", [mol/g]

P_i Permeance of gas "i" through a membrane, [mol/m^2·Pa·s]

P_j Permeance of gas "j" through a membrane, [mol/m^2·Pa·s]

p_{io} Pressure on feed side of membrane for component "i", [Pa]

p_{il} Pressure on permeate side of membrane for component "i", [Pa]

Chapter 1: Introduction

1.1 Overview

Hydrogen production plays an important role in the petrochemical and agriculture industries. Petroleum refineries utilize hydrogen to purify their hydrocarbon streams from sulfur by hydrodesulfurization; this is particularly an important process for Alberta's sulfur contaminated heavy oil from bitumen [1]. Production of ammonia for use as fertilizers also relies heavily on pure hydrogen using the Haber-Bosch process. Not only is the pure hydrogen a major feedstock in many chemical processes, but with increasing concern on climate change, hydrogen is seeing increasing emphasis as a clean zero emissions fuel [1,2,4]. The majority of commercial pure hydrogen is produced by the separation of synthesis gas (syngas). Syngas, which is a fuel gas mixture of predominately H_2 and CO_2, is obtained from either steam reforming of natural gas or by the gasification of coal, municipal waste, and biomass [3,4].

In steam reforming of natural gas, steam is reacted with methane and a nickel based catalyst at high temperatures (700-1100°C) to produce an intermediate mixture of H_2 and CO[5]. In order to produce more hydrogen and reduce CO content, a water gas shift reaction converts the CO into CO_2 yielding syngas. Equations 1-1 and 1-2 show the two general chemical reactions of obtaining hydrogen as syngas from steam reforming [5,6].

Steam reforming of Methane:

$$CH_4 + H2O \rightleftharpoons CO + 3H_2 \qquad\qquad (1\text{-}1)$$

Water gas shift reaction to yield more H_2 and remove CO:

$$CO + H_2O \rightleftharpoons CO_2 + H_2 \qquad\qquad (1\text{-}2)$$

The water gas shift reaction occurs at two temperature stages: a high temperature shift (350-500 °C) and a low temperature shift at (200-250 °C), both using varying catalysts [6]. Separation of CO_2 and generation of pure hydrogen is then achieved by three main technologies: Pressure swing adsorption (PSA), cryogenic distillation, and membrane separations [2].

PSA is commonly employed to purify the H_2 from the shifted syngas stream by adsorbing the carbon oxides in a high pressure chamber over molecular sieve adsorbents (carbon, silica, or zeolite based adsorbents) [2]. PSA separation processes are scalable to low flows, obtain high purity gas, and can operate intermittently; however, they are complex, incur losses when removing impurities from the bed, and operate at ambient temperatures which require cooling of the feed gas [7].

Cryogenic distillation uses freezing temperatures to separate the syngas based on its components' different boiling points [2,7]. The main advantages of this separation include large quantity yields with high purity.

However, cryogenic units are capital intensive, only efficient for large gas flows, and are limited to non-intermittent operations [7].

Membrane separations use selective barriers that separate gas mixtures based on size or solubility under a pressure gradient. They have received much attention for syngas separations due to their potential in achieving high selectivity, scalability, low cost, and possibility of operating at process temperatures (temperatures after water gas shift ranging from 200°C-500°C) in the presence of steam [6]. However, selection of suitable membrane materials remains a challenge.

This study investigates the use of a unique thermally stable deposit of the mineral clinoptilolite, a natural zeolite, as part of a novel composite membrane for syngas separations. Natural zeolites are particularly well suited as membrane materials because they can be selective, thermally stable, chemically resistant, and abundant. Clinoptilolite was mixed within a cement matrix, pressed, and steamed to form a composite membrane. The clinoptilolite has the properties of a molecular sieve and can separate H_2 and CO_2 based on their respective size. While the cement offers an economical and impermeable matrix that is mechanically stable at elevated temperature and is chemically compatible with high partial pressures of steam. Gas permeation measurements were conducted to investigate the composite membranes' performance.

1.2 Zeolites

Zeolites are a class of minerals commonly composed of hydrated crystalline aluminosilicates with porous frameworks having high surface area.

1.2.1 Natural Zeolites

Zeolites were discovered as new mineral species by Swedish mineralogist A. F. Cronstedt in 1756 who also coined the term "zeolite", which is derived from Greek to mean "boiling stone" because when heated in a blowpipe the material frothed [8]. Since then, they were regarded as rare minerals and some were featured as jewelry for over 200 years due to their highly crystalline formations [8,9]; Figure 1 shows an example of a crystalline stilbite zeolite (pink hue) in non-zeolite apophylite (white).

Figure 1: Crystalline Stilbite (pink hue) in Apophylite (white) formation

As more deposits were found and followed by in depth studies, zeolites were discovered to exhibit unique properties such as reversible ion

exchange and molecular sieving (Weigel and Seinhoff 1925) [9]. "Molecular sieving" is a term coined by J.M. McBain in 1932 to describe solid porous materials that can separate molecules by size [8]. Currently, with over 40 naturally occurring types, zeolites are recognized as one of the most exploitable minerals in the world [9].

The majority of natural zeolite deposits are tuffs formed by the deposition of volcanic debris from eruptions on saline alkaline lake basins. Zeolite tuffs formed under these conditions are loosely bound and have porous grain boundaries [9,10]. However, there are deposits of zeolites that have been formed by burial diagenesis known as geomorphic zeolites [9]. Geomorphic zeolites are formed from tuffs that have been buried by layers of geological species under high geothermal temperature and pressure gradients. Unlike zeolite tuffs, geomorphic zeolites have strong grain boundaries that have bounded together; this yields crystalline monoliths with effectively no intercrystalline voids [35]. Clinoptilolite is among the most abundant geomorphic zeolites and is thermally stable above 600 °C which is due to clinoptilolite's Si/Al of 4.25-5.25 [8,40]. Combining its thermal stability, average pore diameter of 0.3-0.5 nm, and defect free properties make geomorphic clinoptilolite an ideal candidate as a membrane material to separate syngas [8].

1.2.2 Synthetic Zeolites

The first synthetic zeolites, "Zeolite A", reported by Milton's 1948 was formed by slow crystallisation of silica-alumina gel in a caustic

environment [8]. Over 100 synthetic zeolites have been developed since, many of which have no natural analogs. Synthetic zeolite crystal sizes tend to be smaller than their natural analog, yet are purer and more uniform making them attractive as catalysts and adsorbents [8,9,11]. Zeolite synthesis processes are described thoroughly by (Cundy) [11].

1.2.3 Zeolite Frameworks

Figure 2 shows three common zeolite frameworks. A detailed look on zeolite frameworks and their properties can be found in (Breck)(Dyer) [8,9].
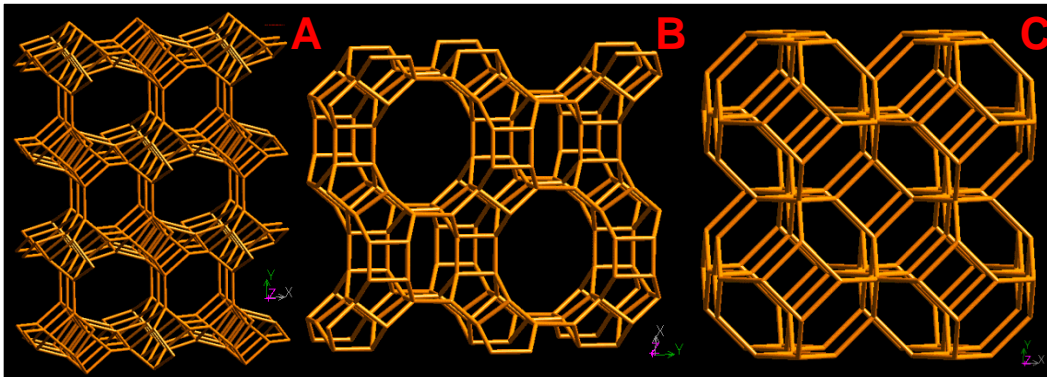
Figure 2: Unit cell frameworks of different zeolite: A) clinoptilolite, B) mordenite, and C) sodalite [12]

Both natural and synthetic zeolites are 3-dimensional crystalline aluminosilicates comprised of corner sharing $[SiO_4]^{4-}$ and $[AlO_4]^{5-}$ forming tetrahedra bridged by oxygens; this infinitely extending crystalline structure forms open frameworks of interconnected microporous channels [8,9]. The valence of the aluminum creates a net negative charge on the framework which is offset by alkali or alkali earth cations that occupy the pores and

channels. The type and quantity of these cations gives rise to many of the unique properties that zeolites are used for. Pore sizes of materials and membranes are classified by IUPAC into three categories: macropores, mesopores, and micropores; each category classifies the range of the pore size diameter as shown in Table 1[13].

Table 1: IUPAC classification of porous material

IUPAC Classification of different porous materials	Pore diameter range (nm)
Macroporous	> 50
Mesoporous	2 – 50
Microporous	< 2

Zeolites' ion exchange ability stems from exchanging the mobile cations within the framework. The pores can hold monovalent or divalent cations such as Li^+, Na^+, and Ca^{2+}. Depending on the exchanged cation, the entire zeolite framework may change its pore size. By changing the cations, it is possible, for some frameworks to modify the pore sizes [8]. Table 2 shows the average pore size ranges for different zeolites; it can be seen that by varying synthetic Zeolite A's cation, a considerable change in pore aperture is exhibited.

Table 2: Common natural zeolites pore size and formulas [8]

Zeolite	Pore Aperture (nm)
Natural clinoptilolite (various cations)	0.4-0.72
Natural sodalite (various cations)	0.26-0.89
Zeolite A (K cation)	0.3
Zeolite A (Na cation)	0.4
Zeolite A (Ca cation)	0.5

Due to their micropore nature, zeolites can behave as molecular sieves either by rejecting molecules too large to fit into the framework or by selectively adsorbing a molecule onto a framework cation. These unique combinations of properties of both natural and synthetic zeolites lead to their widespread use in ion exchange, adsorption, separations and catalysis processes [8,9].

1.2.4 Natural Zeolite Applications

Natural zeolites are particularly attractive to large industrial applications as they are economical, easy to extract, and plentiful. Natural zeolites have been considered as alternative water softening ion exchangers [14]. Junaid et al. used chabazite, a natural zeolite, as a catalyst for oilsands bitumen cracking; offering at alternative solution at lower operating temperatures [15,16,17]. After the Fukushima Daiichi nuclear accident, there has been increasing demand for natural zeolites due to their effective removal of

radioisotopes; Dyer et al. showed the effective uptake of dilute, aqueous radioactive cesium and strontium using the natural zeolite clinoptilolite; [18,19,20]. Natural zeolites have found applications in the livestock industry as nutrient additives due to their detoxifying properties by ion exchange; zeolite inclusion in animal diets yielded healthier livestock and cleaner animal waste [21,22]. The array of industrial applications demonstrates the significant potential of natural zeolite materials.

1.3 Gas Separation Membranes

A membrane is a semipermeable selective barrier that can be used to separate gases or liquid mixtures. Applying a gradient as the driving force across the membrane allows target species to diffuse through.

1.3.1 Historical Development

Membrane science and phenomenon have been studied since the eighteenth century; many of the first investigations looked at using membranes for liquid environment separations and were limited to laboratory scale [23, 24]. By 1960, membrane transport for both gas and liquid separations were fundamentally understood yet remained far from commercial use due to reliability and economic issues [23]. The introduction of the Loeb and Sourirajan membrane process in the early 1960's propelled the development of defect free, high performance reverse osmosis membranes into the commercial space. It wasn't until 1980 that a successful gas separation membrane was pioneered by Monsanto Inc. for separation of hydrogen from off-gas using their PRISM membranes [23]. By

2010, a report by BCC Research estimated that the U.S market for membrane gas separations has grown to $180 million per year, and is forecasted to reach $245 million by 2015 [25].

1.3.2 Gas diffusion through porous membranes

Gas separation membrane processes are defined by diffusion and mass transfer through solids; they can be classified into different types depending on their structure and composition. Membrane performance is determined by two key parameters: permeance and selectivity [23, 24, 26, and 27].

In gas permeation through membranes, the volume molar flux is defined as the flow through the membrane per unit area per unit time and is shown by equation 1-3 for gas component "i" [23]:

$$j_i = \frac{D_i K_i (p_{io} - p_{il})}{l} \tag{1-3}$$

j_i : Volume (molar) flux for gas component "i" at STP, [cm^3/cm^2.s]

K_i : Sorption coefficient for gas component "i" at STP,[cm^3/cm^3]

D_i : Permeate diffusion coefficient for gas component "i"

l : Membrane thickness [mm]

$(p_{io} - p_{il})$: Differential partial pressure for gas component "i" from either side of the membrane with units [Pa]

The product of $D_i K_i$ is the membrane permeability representing the membrane's ability to permeate gas with units [mol·m/m²·Pa·s]. Membrane permeability can be normalized by the membrane thickness and referred to as permeance P_i with units of [mol/m²·Pa·s] [23, 24].

Selectivity "α" is defined as the ability of a membrane to separate two gases; higher selectivities are desirable as they are indicative of good separation. For two gas components "i" and "j", the membrane selectivity "α_{ij}" is unitless and can be calculated by the ratio of each gas's permeances P_i and P_j shown in equation 1-4. (If P_i and P_j were the permeances measured as single gases and not a mixture, the resulting selectivity "α_{ij}" is known as the ideal selectivity)[23].

$$\alpha_{ij} = \frac{P_i}{P_j} \qquad\qquad (1\text{-}4)$$

α_{ij} : The ideal selectivity for gas "i" over gas "j"

P_i: Permeance of gas "i" through a membrane, [mol/m²·Pa·s]

P_j: Permeance of gas "j" through a membrane, [mol/m²·Pa·s]

In this study, membrane performance will be measured by permeance and selectivity.

There are two distinct membrane separation processes: dead-end and cross flow. Figure 3 illustrates the difference between both processes for a porous membrane under a binary gas mixture of different sized gases [23].
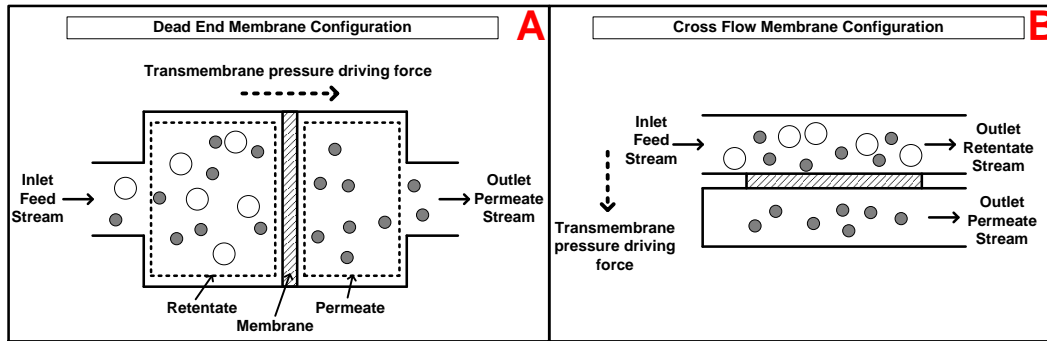
Figure 3: Different membrane separation processes: A) dead end, and B) cross flow. (Adapted from Baker)[23]

Membranes behave as filters that separate the feed components into two streams: the permeate is the component of the feed that diffuses through the membrane, while the retentate is the component that does not. Flow through the membrane from the feed to the permeate side occurs due to a driving force; for gas separations, the driving force is generated by a differential pressure gradient and often referred to as transmembrane pressure. Both dead end and cross flow processes are used to study membrane performance. Although any membrane geometry can be adapted to both processes, cross flow is favored for tubular membranes; however, for disc membranes, a dead end process is more suitable. This study uses a dead end process to measure porous disc membranes for syngas separations.

Gas flowing through a porous membrane diffuses through pores and interconnected voids; the pore sizes dictate the diffusion mechanism [24].

Figure 4 shows a visualization of the three possible gas diffusion mechanisms through different porosity membranes [23].
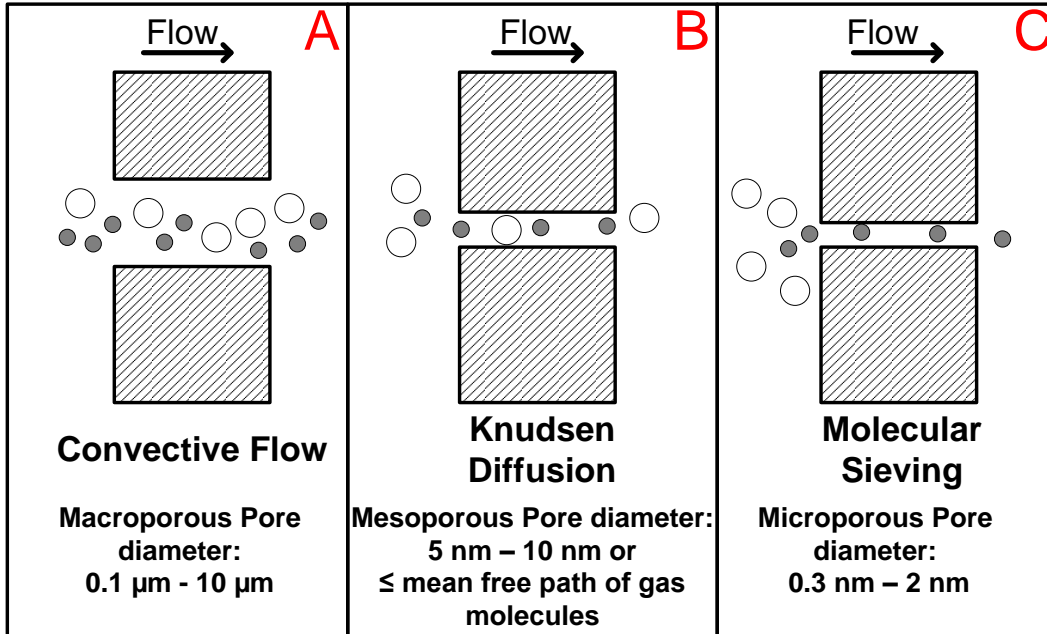
Figure 4: Visualization of gas diffusion mechanisms through porous membranes: A) convective flow, B) Knudsen diffusion, and C) molecular sieving. (Adapted from Baker)[23]

When a membrane has macroporous defects larger than 0.1 µm, a mixture of different sized gases diffuse through the defects by convective flow without any selective separation. This flow does not differentiate between different sized gas molecules and thus is not suitable for gas separation [23,27].

Gas transport mechanism is governed by Knudsen diffusion through a mesoporous membrane with pore diameters from 5 nm -10 nm or smaller than the mean free path of the gases. The mean free path is defined as

the average distance travelled by a gas molecule between successive collisions with another gas molecule [23, 24, 27, 28, 29, 30]. In Knudsen diffusion the gas molecules interact more frequently with the pore walls than with each other. Knudsen diffusion follows Graham's law of diffusion where the transport rate of the gases through the porous structure is inversely proportional to the square root of its molecular weight; lighter gases would have preferential diffusion [23]. This type of diffusion yields a specific limited selectivity known as "Knusden selectivity", shown in equation 1-5.

$$\alpha_{ij} = \frac{\sqrt{M_j}}{\sqrt{M_i}} \qquad\qquad (1\text{-}5)$$

α_{ij} : The Knudsen selectivity for gas "i" over gas "j"

M_i: The molecular weight of gas "i", [mol/g]

M_j: The molecular weight of gas "j", [mol/g]

For single gas studies of H_2 and CO_2, Knudsen selectivity of H_2/CO_2 is calculated to be 4.69. For mesoporous membrane, the maximum selectivity that can be obtained is the Knudsen selectivity.

Microporous membranes have extremely small pore sizes ranging from $0.3 - 2$ nm; gas diffusion through this structure is governed by molecular sieving. Molecular sieving diffusion is complex and incorporates a combination of diffusion in the gas phase and surface diffusion on the pores. This type of diffusion effectively allows the permeation of gases smaller than the pores to pass through while rejecting larger ones.

14

Selectivities obtained under this mechanism should be higher than the Knudsen selectivities [23, 24, 27, 28, 29, 30]. Since the kinetic diameters of H_2 and CO_2 are 0.28 nm and 0.33 nm, to separate them and obtain higher selectivities than Knudsen, microporous membranes are needed.

1.3.3 Porous Hydrogen Separation Membrane Types

Porous hydrogen separation membrane materials are numerous; Table 3 compares three common membrane materials used for molecularly sieving hydrogen from other gases such as CO_2, CO, CH4, etc. [2].

Table 3: Comparison of different porous membrane materials used for hydrogen separation. (Adapted from Phair et al.) [2]

	Polymeric	Glass	Aluminosilicate (Synthetic zeolite)
Permeability	Low-medium	High	Low
Strength	Medium	Strong	Weak
Thermal Stability	Low	Good	Medium-high
Chemical Stability	Low-medium	High	High
Costs	Low	High	Low-medium
Life	Short	Long	Medium-long

Recently, An et al. explored H_2 separation using a new type of membranes machined from monolithic rock sections [31]. The rock fragments came

from a geomorphic deposit of clinoptilolite which was supplied by Castle Mountain Zeolites (Quirindi, NSW, Australia) shown in in Figure 5.

Figure 5: Castle Mountain clinoptilolite mineral with machined discs

Due to the strength of the Castle Mountain clinoptilolite rock sections, it was possible to machine membrane discs directly from the rock fragment. After chemically modifying the surface, the discs demonstrated selective separation for H_2 over CO_2 among other gases and highlighted the potential of natural zeolites as gas separation membrane material [31]. An et al.'s study was conducted with varying temperatures up to 600 °C. The test data demonstrated that the flow through the membrane is predominately through the microporous zeolite framework; the trends across the measured temperature range confirm the high thermal stability of the selected geomorphic zeolite.

Despite being thermally stable and selective towards hydrogen, geomorphic zeolite membranes are limited by the size of the rock

sections. As a result of the mining process, it becomes increasingly difficult to find large uniform rocks that can be sectioned. This poses a scaling limitation for use in industrial processes such as syngas separation.

1.4 Zeolite/Cement Composite Membrane Concept

Increasing interest on zeolite membrane materials for gas separations has led to the development of mixed-matrix membranes (also referred to as composite membranes). A mixed-matrix membrane consists of dispersing a zeolite particle phase within a polymer matrix [23]. Mixed-matrix membranes benefit from zeolites' selectivity and polymers' low cost [23, 32, 33]. Figure 6 illustrates the composite membrane concept and how it can be applied to separate H_2 and CO_2 based on size.

Zeolite Crystals

Dense Matrix

H_2

CO_2 is Rejected by the matrix and zeolite crystals

CO_2

H_2 passes through zeolite channels but not the matrix

CO_2

H_2
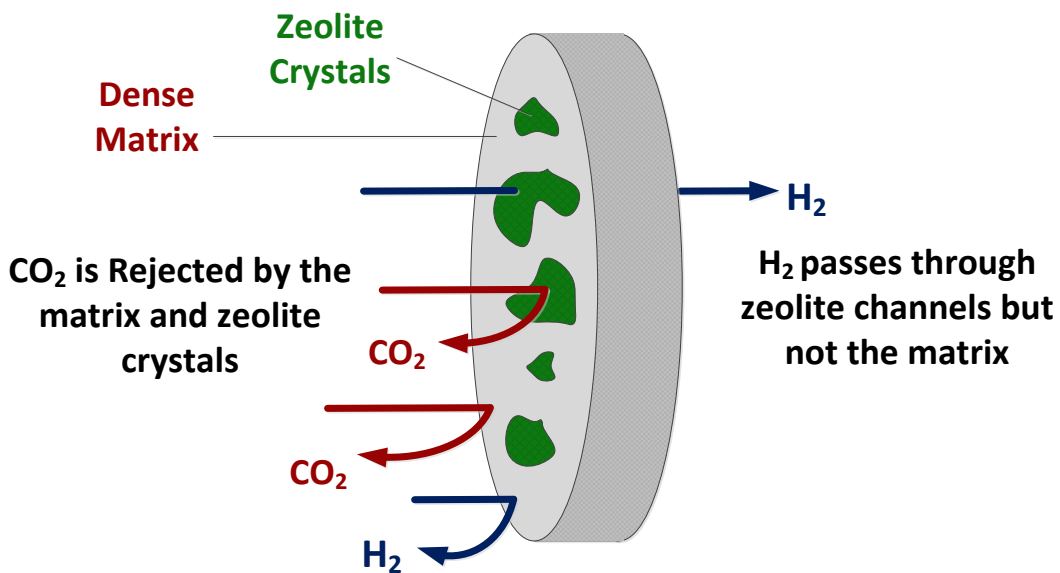
Figure 6: Composite membrane concept for H_2/CO_2 separation

In this study, we adopted the mixed-matrix membrane concept to address the scalability limitations of the geomorphic membranes reported by An et al. However, instead of using a polymer matrix, natural clinoptilolite crushed powder was embedded in a cement matrix to form a membrane. For H_2 and CO_2 separation, a composite membrane should exhibit microporosity and have an absence of intercrystalline defects to allow molecular sieving to occur.

Cement is a widely used hydraulic binder and is the primary ingredient in concrete mixtures for construction (buildings, pavements, etc.). Dry fine powdered cement reacts with water (hydration reaction) to form new phases that precipitate steadily developing strength and curing over long periods [34]. Although after exposure to water, cement continues to gain strength after several years, 28 days is regarded as the practical time necessary for a substantial percentage of hydration to occur [34]. Pozzolanic materials are supplementary cementitious materials that are used as additives to Portland cement blends; they are predominantly composed of siliceous or siliceous and aluminous materials [35,36]. Precedence exists for the inclusion of natural zeolites as pozzolanic materials into Portland cement, underlying zeolite/cement compatibility [35,37,38,49]. Cement was chosen as a matrix due to zeolite compatibility and higher thermal stability than most polymers (up to 500 °C), and potential for steam resistance, which is required for operating at syngas process temperatures [6,39, 52].

In this study, composite membranes were prepared by dry pressing a zeolite/cement mixture into discs which were subsequently steamed and tested. Not only does a dry pressed disc offer flexibility in fabrication, but also offer a solution to scalability and ability to compare with previous rock section discs.

The zeolite selected for this work was clinoptilolite to maintain similar selectivity as An et. al. Cement was selected as the matrix material since its multidirectional crystal growth (after hydration) may heal defects as it bonds with the chemically compatible zeolite. However, the cement matrix must demonstrate impermeability toward CO_2 while allowing the H_2 gas to permeate through it and the zeolite crystals. The combination of an impermeable matrix and the clinoptilolite particles should allow us to fabricate membranes that approach the performance of geomorphic rock sections.

Chapter 2: Materials and Methods

This chapter introduces the material characterization, composite membrane preparation, and instrumentation involved in measuring membrane integrity and performance.

2.1 Material Characterization

2.1.1 St. Cloud Clinoptilolite

The natural zeolite used in the study was clinoptilolite from the "Ash Meadows" deposit of St. Cloud (Winston, New Mexico, US), referred to as zeolite interchangeably throughout this study. It was purchased as ground powder passed through a 325 mesh sieve (particle size< than 45 µm) [41].

Since the zeolite will be crushed and embedded in a matrix, the requirement that the clinoptilolite be obtained from a geomorphic deposit with no intercrystalline voids is not needed. The Ash Meadows deposit is loosely bound tuffs and not geomorphic. However, it was chosen as a geomorphic substitute since it matches the geomorphic clinoptilolite's high thermal stability, high purity, and is commercially available. Ash Meadows clinoptilolite has a Si/Al ratio of 5.1 yielding a thermal stability of up to 650 °C [41].

X-ray diffraction (XRD) was employed to verify the purity of the clinoptilolite powder. XRD is a technique that determines the physical and chemical properties of an unidentified crystalline material by analysing the diffraction pattern from an incident X-ray beam [42]. Crystalline materials

scatter x-rays according to Bragg's law and patterns are collected as scattered intensity versus twice the incident beam angle. The relative positions of the peaks are unique to each crystalline material and when measured across a range of angles, provide a fingerprint pattern that can be used to identify the material [42].

Figure 7 reveals the X-ray diffraction pattern for Ash Meadows clinoptilolite matching a calcium-clinoptilolite from the mineral database and validating the 80 wt% purity reported by the supplier [41]. The remaining 20 wt% can be attributed to the unassigned peaks as quartz or other impurities. Having a predominantly pure zeolite composition ensures a high active component in the composite membrane.
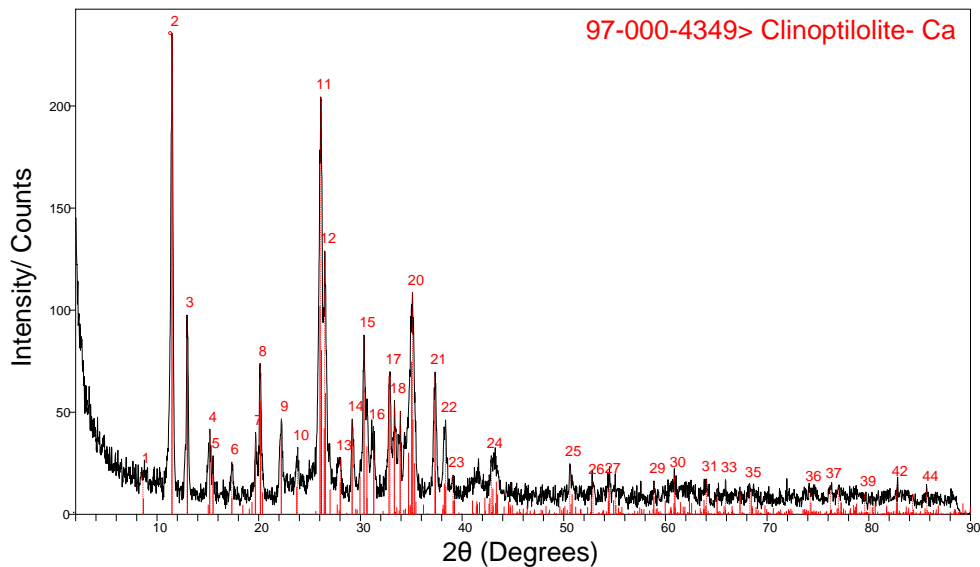
Figure 7: XRD pattern for Ash Meadows clinoptilolite

Dynamic light scattering is an instrument that calculates the particle size distribution of a powder by analyzing the laser scattered diffraction pattern off of a small quantity suspended in water [43]. Dynamic light scattering was used to specify the fineness of both zeolite and cement powders. Particles were assumed to be spherical by the analysis software with the diameter D_{50}, describing 50% of the particles' sizes. The Ash Meadows clinoptilolite D_{50} was identified as 6.01 μm (see Figure 8).
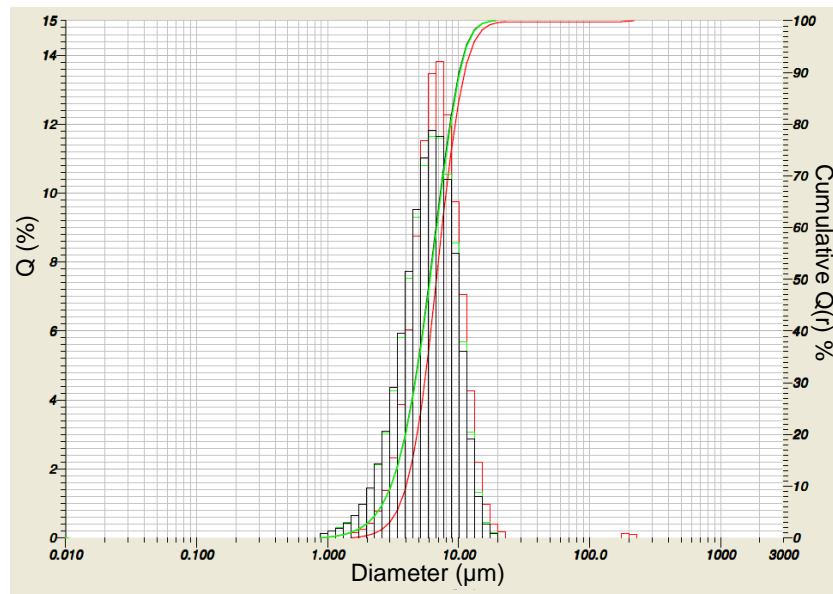
Figure 8: Particle size distribution for Ash Meadows clinoptilolite

2.1.2 Portland Cement

The cement used in this study was type CEM I (European Standard EN 197-1); it is also known as "Ordinary Portland Cement" or "general use cement". Table 4 shows the major chemical constituents of cement; while the minor remaining constituents may contain un-combined lime and

magnesia along with alkalis and minor amounts of gypsum/ potassium/ sodium oxide.

Table 4: Common cement compounds [34,44]

Compound name/ formula	Wt %
Tricalcium Silicate/ Ca_3SiO_4	42-65
Dicalcium Silicate/ Ca_2SiO_5	10-30
Tricalcium Aluminate/ $Ca_3Al_2O_6$	0-17
Tetracalcium Aluminoferrite/ $Ca_4Al_2Fe_2O_{10}$	6-18

When hydrated, cement's setting time is proportionally dependent on the particle size. The setting time is reduced significantly with finer cement particles [34]. This mechanism is related to the specific surface area available for the hydration to occur. It can be problematic for concrete processing if the cement is ultrafine (<1 μm) and cures quickly without providing sufficient time for mixing and handling. Therefore, the particle size distribution of any general use cement must be across a wide range of small particle sizes in order to control setting time (<50 μm). Having a variety of particle sizes generates a reasonable setting time and also enhances cement strength. The characteristic breadth of cement's particle sizes was observed as a bimodal distribution when dynamic light scattering was conducted [45,46,47]. Figure 9 shows the particle size

distribution for our cement; as assumed earlier, the $D_{50} = 6.97$ µm was used to describe the average particle size.
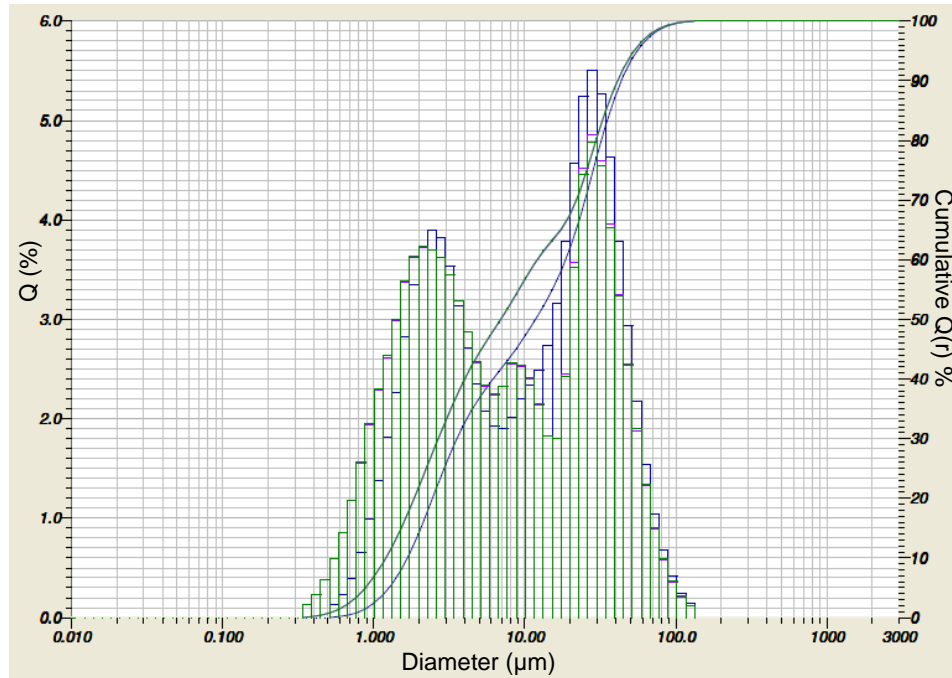
Figure 9: Particle size distribution for cement

2.2 Composite Membrane Preparation

A composite membrane was prepared by mixing a homogenous powder of Ash Meadows clinoptilolite with cement and then pressing it into a disc that was subsequently steamed. After steaming, the resulting disc is considered a "membrane" and the sample was allowed to dry inside a dehumidified container.

2.2.1 Green Body Pressing

The first step in a composite membrane preparation was to completely blend Ash Meadows clinoptilolite and cement powders in an automated

inversion blender for eight hours (Glen Mills Inc. Turbula® T2F Shaker-Mixer). A weight of 2.20 g of the mixture was then distributed into the die as shown in Figure 10. The plenum space in the die was predetermined by a specific thickness using measured plates. The die was then pressed using an axial hydraulic press at 50 kN for 1.5 minutes. After pressing, 27 mm disc green bodies with a thickness ranging from 1.8 mm to 2.2 mm depending on zeolite/cement ratio were recovered. The term "green body" will be used to describe the pressed discs before steaming. Figure 11 highlights the green body pressing steps used. Packing fine zeolite and cement powders would increase contact area between both components; when water is applied by steaming, numerous grain boundaries could be formed yielding stronger zeolite/cement binding.
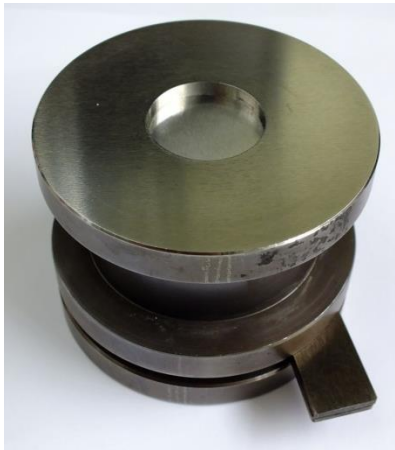
Figure 10: Stretched carbon steel die used for packing powder mixtures into 27 mm discs

1.Distribute powder   **2. Cover die and Press**   **3. Recover green body**
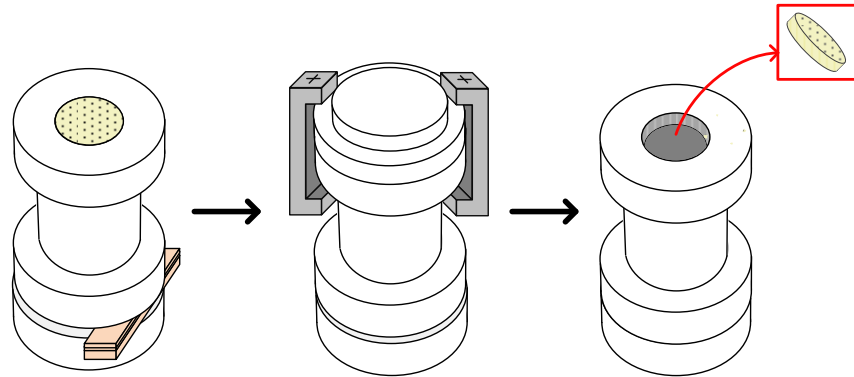
Figure 11: Green body pressing preparation.

2.2.2 Steaming

The green body strength of the recovered discs after pressing is low and unsuitable for membrane testing. Thus, a method to cure the cement to gain strength is necessary. Immersion of the discs in liquid was not viable as the discs disintegrated; steaming was observed to effectively cure the green discs and is reported as an alternative method of hydrating cement [53]. The process of steaming green bodies can result in disc warping (curving). Therefore, we explored three different steaming configurations (autoclave, stack, and flat bath steaming) to determine which technique yielded the flattest and strongest membrane discs.

2.2.2.1 Autoclave Steaming

As the first steaming configuration, autoclave steaming was carried out using a 250 mL Teflon liner inside a carbon steel pressurized vessel (model is D3-1420 from the manufacturer Berghof). A single membrane was placed on top of a hollow ceramic cylinder with 15 ml of deionized

water at the bottom (Figure 12). The autoclave was placed in an oven at 200 $^\circ$C for eight hours.
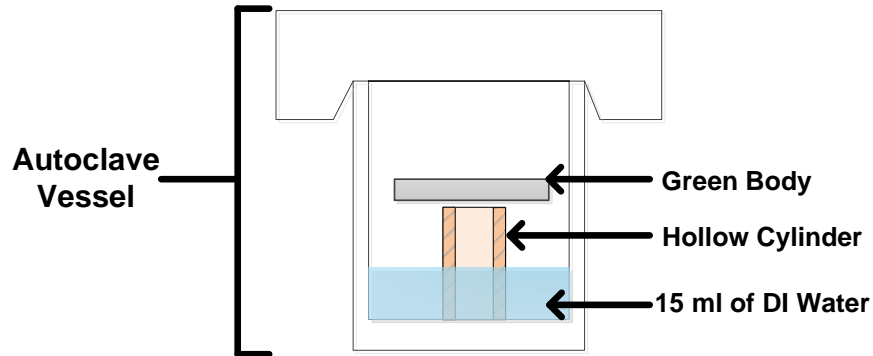
Figure 12: Schematic of autoclave steaming setup

The autoclave hydrothermal treatment yielded cured discs that were brittle and crumbled upon handling (see Figure 13). The consistently low strength was independent of mixture ratios and therefore this steaming technique was abandoned.

Figure 13: Cracked membrane prepared using autoclave steaming

2.2.2.2 Stack Steaming

The second steaming technique looked at focussing steam onto a green body via a chimney stack. As can be seen from Figure 14, a hollow stainless steel stack was placed over a flask with pins that support the

green body. The flask was filled with 200 ml of deionized water, and heated on a plate set at 200 $^{\circ}$C with stirring at 200 rpm. The green bodies were steamed for three hours per day for three days with the deionized water replenished daily.
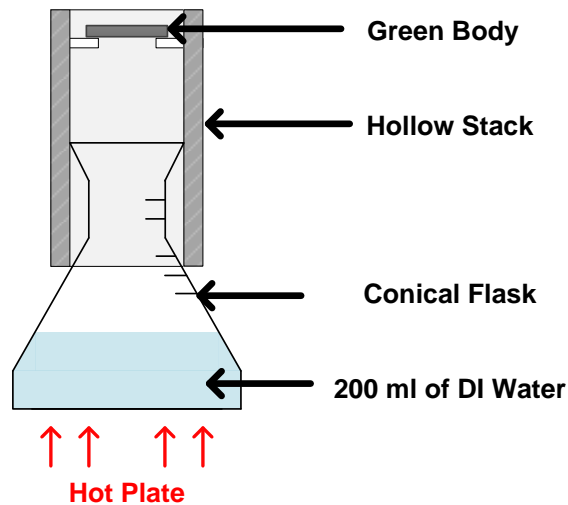
Figure 14: Schematic of stack steaming setup

Membranes prepared by stack steaming were significantly stronger than those made using autoclave steaming. However, as shown in Figure 15, stack steaming would steam one side of the membrane too quickly and the resulting disc would be distorted which was apparent in their curvature. Rather than attempt to optimize the conditions to eliminate curvature, an alternate bath configuration was used.

28

Figure 15: Curved membrane obtained using stack steaming

2.2.2.3 Flat Bath Steaming

The third technique utilizes a flat bath steaming setup as shown in Figure 16. Green bodies were placed on top of a stainless steel "wire mesh 10" above a 250 ml beaker. As with the other techniques, the beaker was filled with 200 mL of deionized water, magnetically stirred at 200 rpm and heated on a hot plate set to 200 °C. This configuration allowed for multiple membranes to be steamed simultaneously. The green bodies were steamed for eight hours daily for three days. To avoid disc curvature, ensure water saturation, and evenly distribute the steam, membranes were flipped every 30 minutes and the beaker was replenished every two hours.
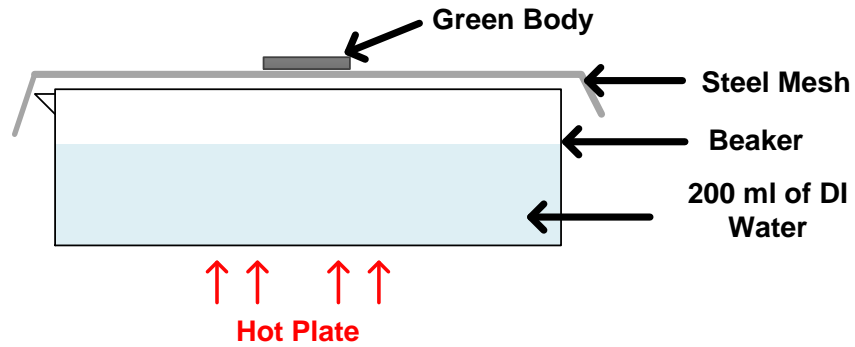
Figure 16: Schematic of the flat bath steaming setup

Membranes prepared by flat bath steaming did not exhibit any curvature and were considerably stronger than the ones prepared with the other steaming techniques. Figure 17 shows a membrane that lacks curvature due to flat bath steaming beside a membrane that is curved due to chimney steaming. Flat bath steaming was therefore adopted as the primary curing technique for the membrane preparation recipe. Figure 18 shows a membrane with a 33 wt% zeolite in cement composition, prepared using a flat bath steaming.

Figure 17: Comparison of two membranes: (Left) flat membrane prepared using flat bath steaming, and (Right) membrane prepared using stack steaming showing curvature

Figure 18: 33 wt% zeolite membrane after flat bath steaming

2.3 Composite Membrane Testing Instrumentation

2.3.1 Microscopy of Membrane Surface

A scanning electron microscopy (SEM) Ultra55 was employed to observe membrane surface morphology at different magnifications. Energy dispersive X-ray spectroscopy (EDS) identified changes in composition from an area with zeolite agglomeration to pure cement.

A Keyence VK-9710 Confocal Scanning Laser Microscope (CSLM) was used to obtain membrane surface topography information. A CSLM uses points to create a 3D reconstructed image from different sectioned magnification levels. It was useful in identifying wells on the membrane surface, which were found to be zeolite agglomerate regions by EDS.

2.3.2 Air Leakage Testing (ALT) Setup

Air Leakage Testing (ALT) was selected to screen composite membranes with low air leakage rates. The ALT setup consisted of a flange, vacuum pump, and an Integra DDV leak test system (Dr. Wiesner Steuerungstechnik, Germany). Figure 19 illustrates the schematic for the

ALT setup while Figure 20 shows the flange module and the interior silicone sealing configuration. The testing area was 3.14 cm^2. A membrane was sealed inside the flange and subjected to a vacuum pressure of 98,000 Pa (980 mbar) at 25 $^\circ$C. The vacuum was then switched off and the system was allowed to equilibrate while the Integra monitors the vacuum loss through the porous membrane.

The Integra system uses the differential pressure decay method to calculate the specific air leakage rate in [Pa·L/ cm^2·s] [50]. Membranes with low specific air leakage rates < 0.05 Pa·L/ cm^2·s were considered microporous, or with acceptable defects. On the other hand, membranes with specific air leakage rates ≥ 0.05 Pa·L/ cm^2·s were excluded from further testing as they were considered to have high porosity or defects.
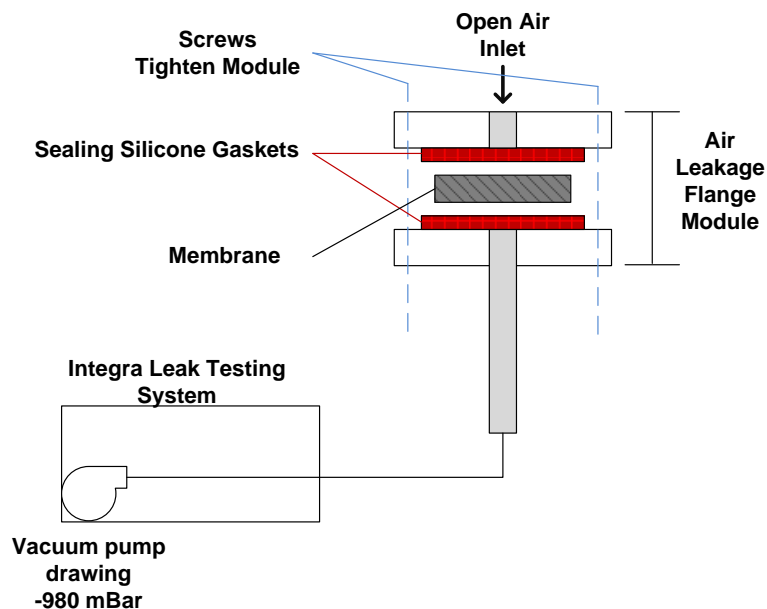
Figure 19: Schematic of Air Leakage Test setup with Integra Leak Testing System

Figure 20: Air Leakage Test flange module with the stainless steel reference membrane

2.3.3 Gas Permeation Measurement (GPM) Setup

Gas Permeation Measurement (GPM) was the final test conducted on our composite membranes after ALT. As opposed to the screening of ALT, GPM quantifies the membrane performance by measuring the gas permeance across a membrane at a fixed differential pressure. Using the measured flux, area, and thickness of the membrane, permeance and selectivity can be calculated using the formulas shown in section 1.3.2. Permeance, given in [mol/m^2·Pa·s], is the primary metric obtained from GPM. Our objective was to obtain composite membranes that have both a high permeance (on the order of 10^{-6} mol/m^2·Pa·s) and H2/CO$_2$ selectivity above Knusden at 4.69.

The GPM utilizes a pressure gradient across a membrane inside a flange to drive gas from the feed side to the permeate side. The feed side contains the inlet gas, while the permeate passes through the membrane; rejected gas by the membrane is known as the retentate and is vented.

This was a single gas study measuring H_2 and CO_2 permeances under 1-4 bar differential pressure (1 bar increments) at 25 $°C$. The entire system was connected with Swagelok stainless steel tubing and fittings. Gas cylinders were provided by the Linde Group. Figure 21 shows a schematic of the membrane flange; the membrane was sealed between two silicone O-rings. The testing area was 3.14 cm^2.
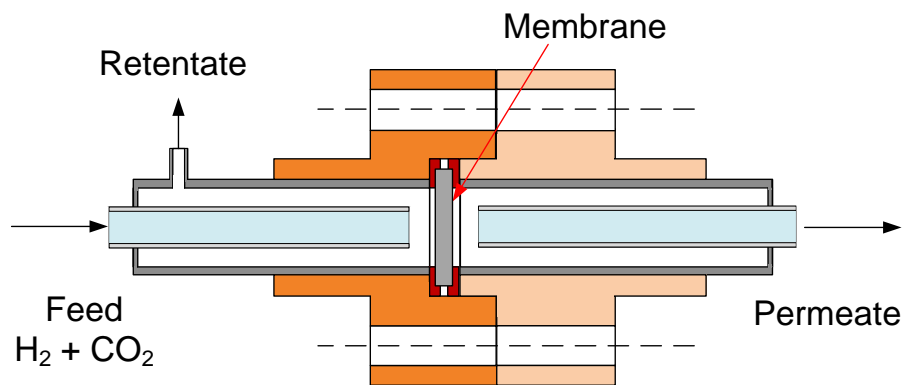
Figure 21: Schematic of GPM membrane flange and gas flow

Figure 22 shows the process flow diagram of the GPM setup. Each mass flow meter (MFM) was calibrated to each gas (H_2 and CO_2); the lowest detectible flow was 0.03 ml/min. MFM 1 measured the feed side flow rate while MFM 2 measured the permeate flow rate. A Brooks 5866 pressure controller was used to deliver the desired pressure into the membrane flange; the controller could deliver up to 4 bar differential pressure across the flange. The flange was purged between runs to vent off any residual gases in the tubing. Hydrogen was tested first and followed by carbon dioxide. For each run, once the system reaches steady state at the

desired differential pressure, data were continuously logged for 10 minutes.

Figure 22: Process flow diagram for the Gas Permeation Setup

Chapter 3: Results and Discussion

3.1 Demonstration of an Impermeable Cement Membrane

This section demonstrates the viability of cement as an impermeable matrix material. Composed of 100% cement, M300 was the first membrane that demonstrated impermeability toward CO_2. It was prepared using the composite membrane preparation method outlined in Chapter 2 without the addition of the zeolite powder. The membrane was tested by both ALT and GPM (at 4 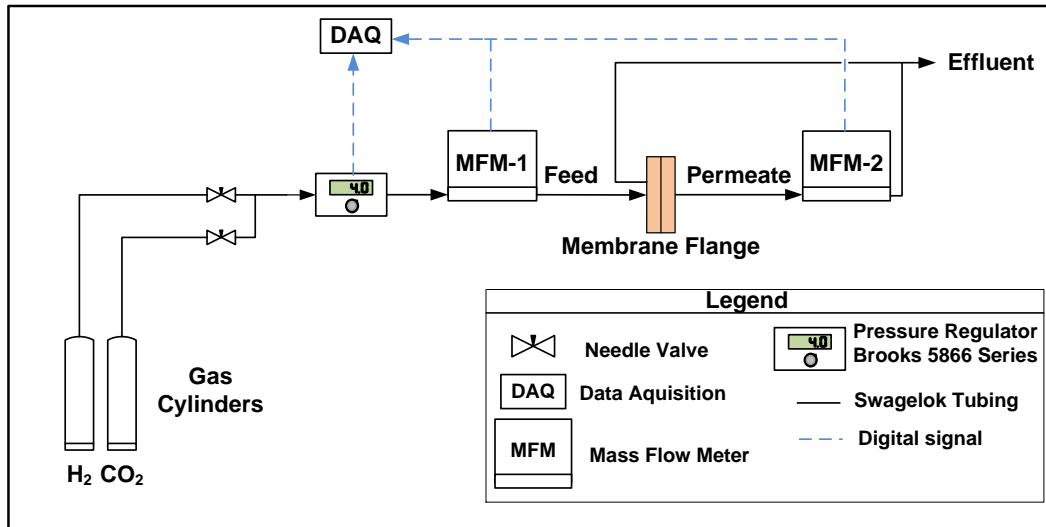bar differential pressure) immediately after being prepared and again after 26 days. As mentioned in section 1.4, 26 days is an ideal time to observe any changes to the cement due to curing time. The resulting data is shown in Table 5.

Table 5 shows that the 100% cement membrane at 0 days had a specific air leakage rate of 0.022 Pa·L/cm^2·s; which is within the acceptable defect range defined by ALT (<0.05 Pa·L/cm^2·s). After 26 days, the air leakage rate dropped to 0.013 Pa·L/cm^2·s indicating a decrease in porosity. Also after 26 days, the GPM showed that H_2 and CO_2 permeance dropped below the lowest detectible limit. This reduction in permeance for air, H_2, and CO_2 indicates a change in the microstructure that has a direct positive effect on gas permeance. This structural change is reflected in the loss of permeability for all gases once the cement is cured. Thus, the effect of cement impermeability over time is of net benefit to the zeolite-cement system.

Table 5: Pure cement membrane M300, ALT and GPM vs. time

Membrane M300 (100% Cement)	0 Days	26 Days
ALT - Specific air leakage rate [Pa·L/ cm^2·s]	0.022 ± 1.4%	0.013 ± 3.8%
GPM - H$_2$ Permeance [mol/m^2·Pa·s]	1.8E-08 ± 0.5%	non detect
GPM - CO$_2$ Permeance [mol/m^2·Pa·s]	1.4E-09 ± 7%	non detect

3.2 Mixing Effects and Zeolite/Cement Connection

While maintaining the pressing and steaming steps described in Chapter 2, this section compares membranes that had their zeolite-cement powder incompletely mixed by hand for short periods (5 minutes), with those that had their powder completely mixed by an automated inversion blender for longer periods (eight hours). The effect of incompletely/completely mixing on the porosity of composite membranes was examined by ALT. SEM and CSLM imaging was also used to compare surfaces in both cases.

Membrane M318, prepared by incomplete mixing, was compared to M327, prepared by complete mixing; both were composed of 33 wt% zeolite. Figure 23 shows a visual comparison between the two. Agglomerated white spots were visible on the incompletely mixed disc, while completely

mixed disc showed a homogeneous surface. It was also found that completely mixed membranes were consistently stronger due to better packing when compared to the incompletely mixed ones.
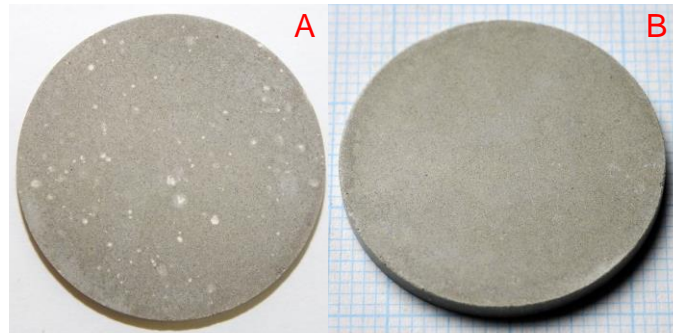
Figure 23: Comparison between A) Incompletely mixed M318, and B) completely mixed M327

Using SEM and EDS, the white agglomerate spots formed by incomplete mixing were examined at high magnification to identify composition (Figure 24 and Figure 25). It was observed by EDS that the elemental composition changes from the center of the spot to the perimeter. Figure 25 shows the EDS points (spectrums 1, 2, 3, and 4) and their corresponding locations, while Table 6 summarises the distinguishing elemental peaks of each point. Peaks of Si, Al, Na, and K were prominent in spectrums 2, 3, and 4 reflecting clinoptilolite's aluminosilicate framework. The low Al yet high Ca peaks reflect the cement composition that surrounds the zeolite agglomerate at spectrum 1. Thus, the white spots resulting from incomplete mixing were identified as agglomerates of zeolite particles.
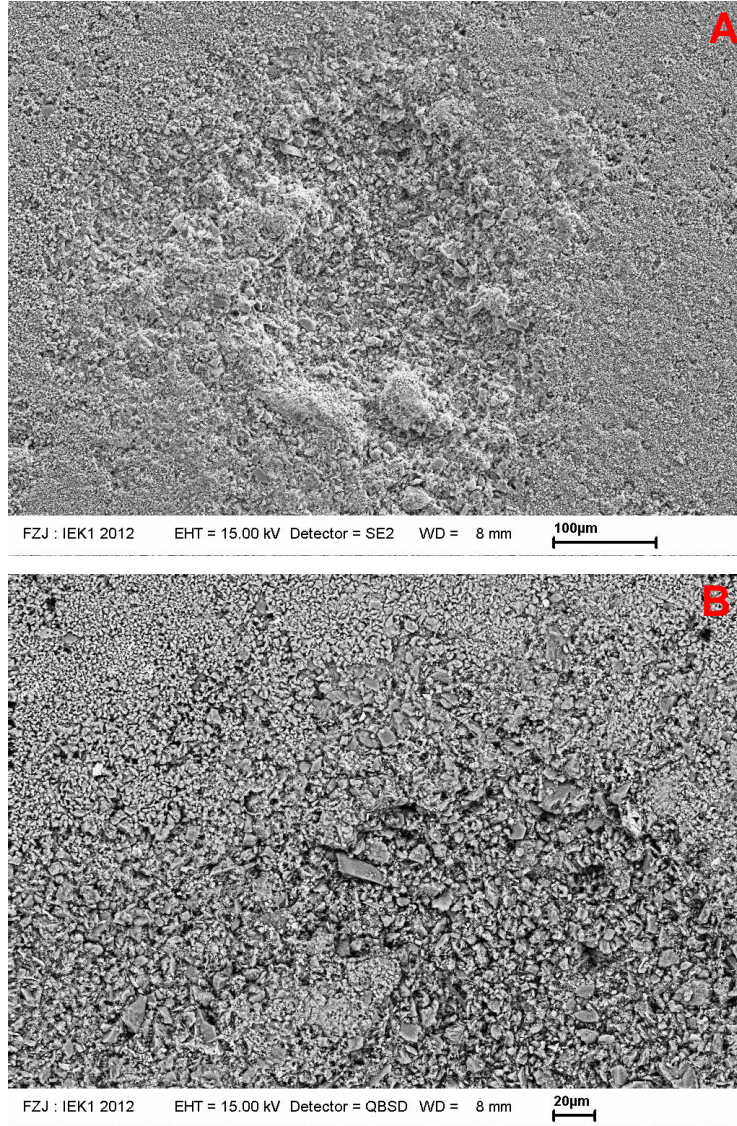
Figure 24: SEM micrographs showing different magnifications of white spots
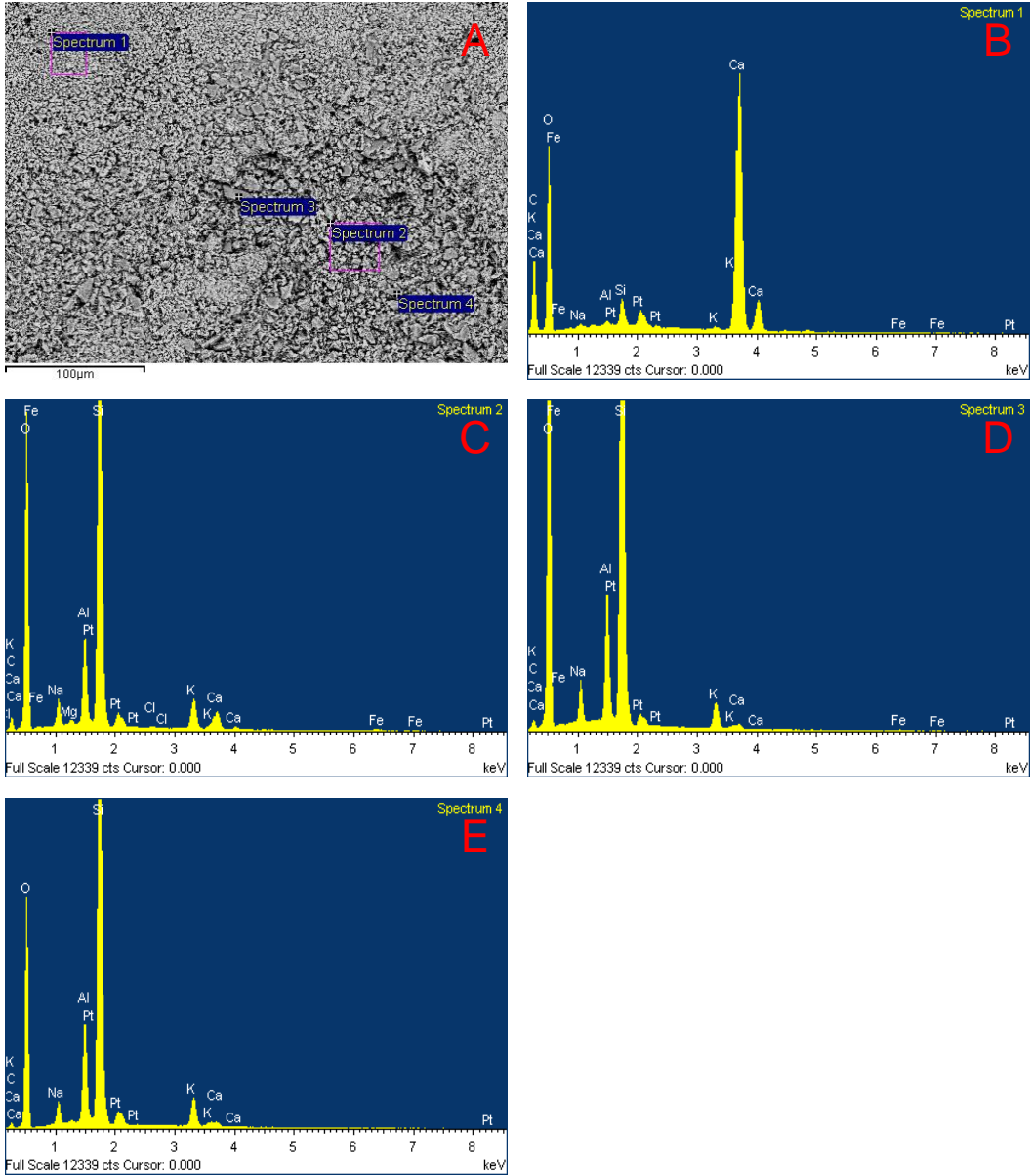
Figure 25: EDS point analysis across the center to the perimeter of the agglomerate spots: A) EDS point locations, B) Spectrum 1, C) Spectrum 2, D) Spectrum 3, and E) Spectrum 4

Table 6: Summary of EDS elemental composition

EDS point	Location with respect to white agglomerate	Elements detected (peaks)	Characteristic Material
Spectrum 1	Outside agglomerate	High: Ca, O, Low: Si, Al	Cement
Spectrum 2	Near center	High: Si, Al, O Low: Na, K	clinoptilolite
Spectrum 3	Perimeter	High: Si, Al, O Low: Na, K	clinoptilolite
Spectrum 4	Center	High: Si, Al, O Low: Na, K	clinoptilolite

CSLM was conducted to measure the surface topology of the zeolite agglomerate spots (see Figure 26). The spots showed a depth in elevation forming zeolite wells. Figure 27 shows the dimensions of an agglomerate well, revealing a horizontal length of ~450 µm and a ~150 µm depth.

Figure 26: Laser microscopy imaging showing agglomerate well

Figure 27: Profile of zeolite agglomerate well and dimensions

The presence of these wells indicates a zeolite/cement connection at the wells' perimeter but not at the center where zeolite/zeolite connections predominate. The wells were formed due to ejected zeolite particles which lacked the ability to adhere to one another.
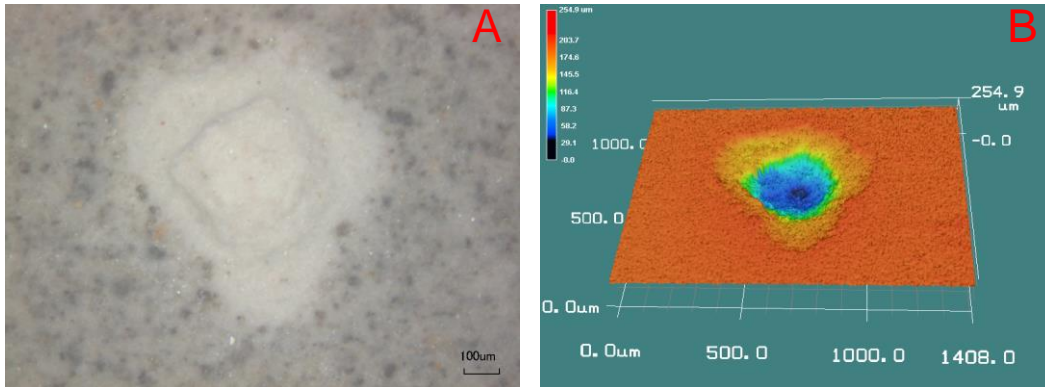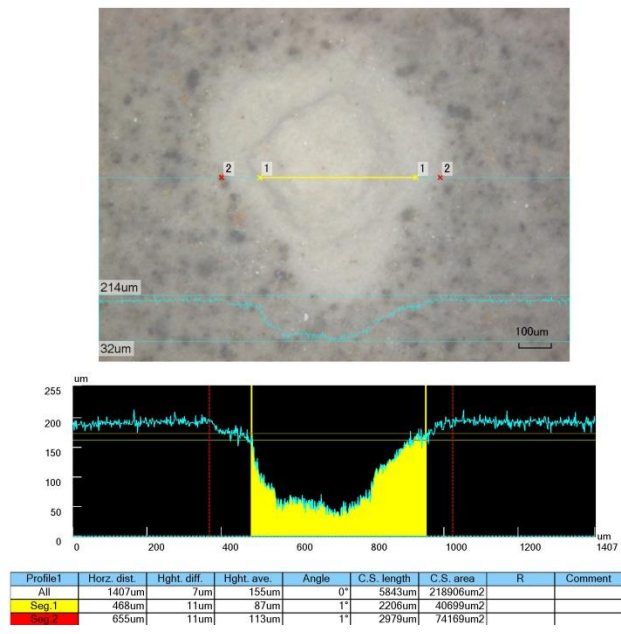
Not only does incomplete mixing disrupt the distribution of zeolite within the cement matrix, but considerably affects porosity and increases defects. This is apparent when comparing the specific air leakage rates of incompletely mixed and completely discs. Table 7 highlights the increase in leakage rate of incompletely mixed disc well beyond the ALT criteria of 0.05 $Pa \cdot L/cm^2 \cdot s$ which was met by the completely mixed disc. The size of the agglomerates (on the order of ~400 μm) in incompletely mixed membranes is large when compared to gas molecules and the particles size of the individual zeolite and cement particles (D_{50}= 6.01 μm and 6.97 μm). When a membrane is incompletely mixed, the zeolites are not fully connected to the cement giving gases a pathway to percolate easily, which explains the high leakage rate obtained by the incompletely mixed disc M318.

Table 7: Mixing comparison of Air Leakage Rate for M318 and M327

Membrane Description	Specific Air Leakage Rate [$Pa \cdot L/cm^2 \cdot s$]
M318: Incomplete mixing, 33 wt% zeolite	0.186 ± 0.7%
M327: Complete mixing, 33 wt% zeolite	0.023 ± 3.1%

In summary, the surface characterization and ALT testing verifies that the clinoptilolite powder is chemically compatible with the cement and strong grain boundaries are formed when the two components are in contact.

The data also demonstrates that the degree of mixing directly influences the porosity of the membrane. It was demonstrated that cement as a matrix strongly bonds to the zeolite and seals defects that would otherwise allow air to percolate through without any resistance.

3.3 Effect of Varying Zeolite Composition on Porosity and Strength

This section explores the effect of varying the zeolite content in a completely mixed membrane on porosity and strength; the ratios examined were 0, 15, 33, 40, 50, 67, and 88 wt% zeolite in a cement matrix.

Despite maintaining a consistent preparation method, it was found that adding more zeolite content above 33 wt% zeolite yielded weaker membranes with porosity beyond the ALT criteria. As discussed in Chapter 2, a membrane with a specific air leakage rate higher than 0.05 $Pa·L/cm^2·s$ was considered non-microporous.

Figure 28 presents the specific air leakage rate data vs. membrane wt% zeolite (each point is an average of three runs for selected membranes). Figure 28 shows that only 0, 15, and 33 wt% zeolite ratios met the ALT criteria for membrane microporosity. Ratios up to 50 wt% zeolite did not show much error in measurement due to the ALT setup being able to draw vacuum consistently. However, for a 67 wt% zeolite membrane, the error highlights the instrument's limitation to draw a vacuum for more porous

material. The membrane with 88 wt% zeolite was not able to seal due to the high porosity and thus could not yield a reliable ALT value.
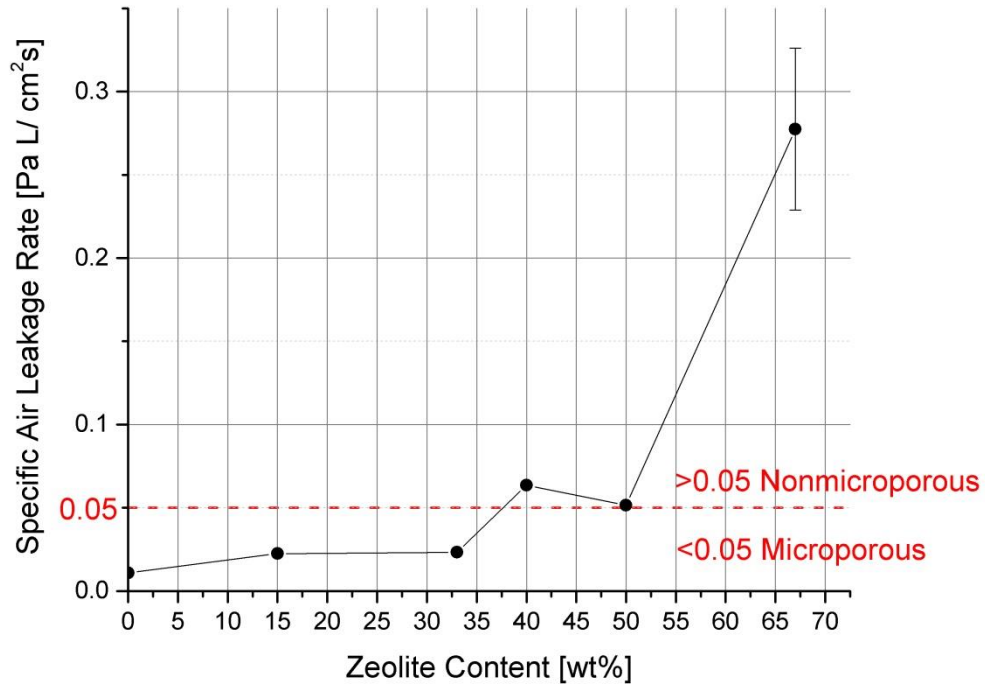

Figure 28: Specific Air Leakage Rate vs. increasing wt% zeolite (0,15,33,40,50,67 wt% zeolite)

Moreover, membranes with zeolite content above 33 wt% zeolite were weaker and cracked more frequently upon fabrication or under 4 bar GPM testing. Figure 29 shows the different zeolite content explored and their mechanical stability.
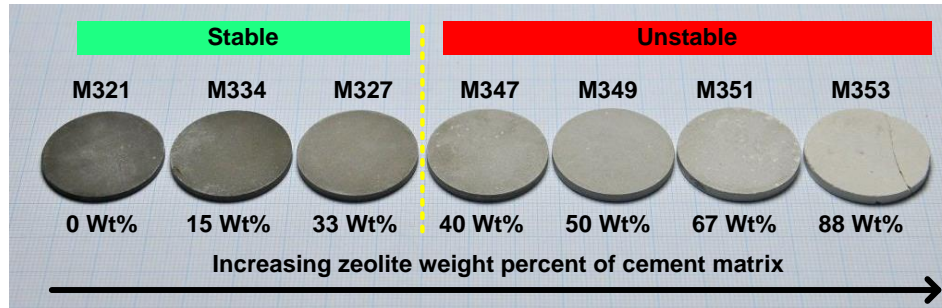
Figure 29: Effect of increasing zeolite content on membrane strength

In summary, only membranes with 0, 15, and 33 wt% zeolite demonstrated strength to withstand the 4 bar differential pressure requirement of GPM testing. Since the GPM testing was the only test that quantified the separation performance of the various compositions, discs that could not be integrated into the test system could not be included in the study.

3.4 Air Leakage Testing Results

A batch of 18 composite membranes made up of six replicates of each of the three stable ratios (0, 15, and 33 wt% zeolite) were prepared and tested by ALT and GPM.

As described in Chapter 2, prior to testing the membranes for permeance under GPM, the 18 membranes were screened for defects/porosity using the air leakage setup.

Figure 30 presents the average specific air leakage rates for all 18 membranes with varying zeolite fractions. Six duplicate membranes composed of 0 wt% zeolite gave an average specific air leakage rate of

46

0.028 Pa·L/cm^2·s with a standard deviation of 5.4%. The membranes composed of 15 wt% zeolite averaged at 0.018 Pa·L/cm^2·s and a standard deviation of 4.3%. The 33 wt% zeolite membranes were 0.015 Pa·L/cm^2·s at 4.7% standard deviation. When compared to Figure 28, the decreasing trend in porosity in Figure 30 shows that the higher porosity in Figure 28 exhibited for ratios higher than 33 wt% zeolite are due to mechanical stability. It can be seen that the 18 membranes met the ALT criteria (< 0.05 Pa·L/cm^2·s) with a maximum of 5.7% standard deviation. Therefore they were suitable for GPM performance testing.
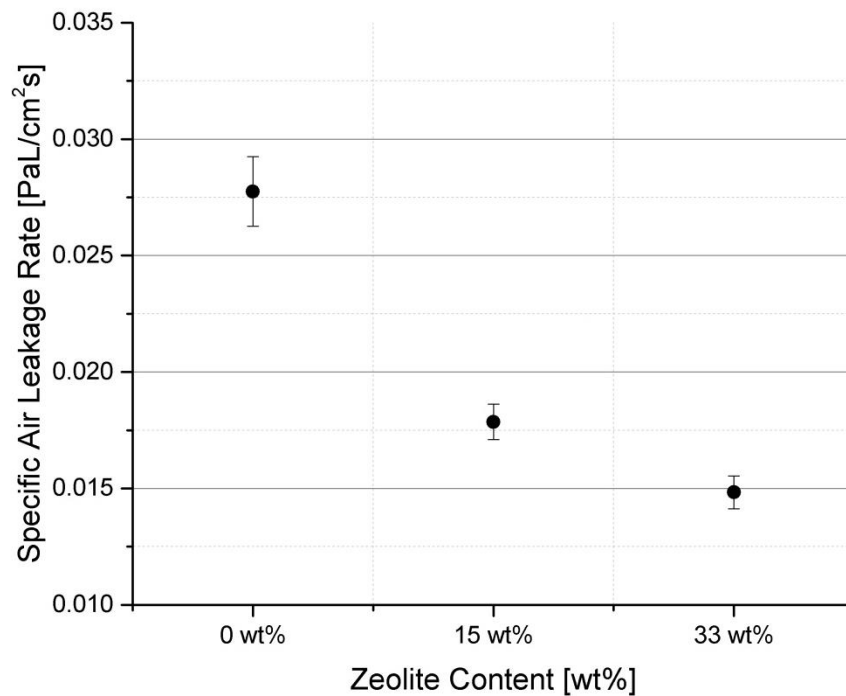
Figure 30: Air Leakage Rate vs. wt% zeolite for average values for 18 membranes at 25 $^\circ$C

3.5 Gas Permeation Measurement Results

3.5.1 GPM for 18 Membranes at 1 Bar differential pressure

The H_2 and CO_2 gas permeances were measured for all 18 membranes using the GPM setup at 1 bar differential pressure and 25 °C; the results are presented in Figure 31. The measured flows for the permeance were well above the detection limits of the GPM flow meters' sensitivity and therefore were not considered noise. The H_2 average permeances for membranes composition of 0, 15, and 33 wt% zeolite were 4.0E-9, 2.5E-9, and 3.6E-9 mol/m^2·Pa·s respectively. While the CO_2 average permeances were 4.3E-10, 7.9E-10, and 1.7E-10 mol/m^2·Pa·s.
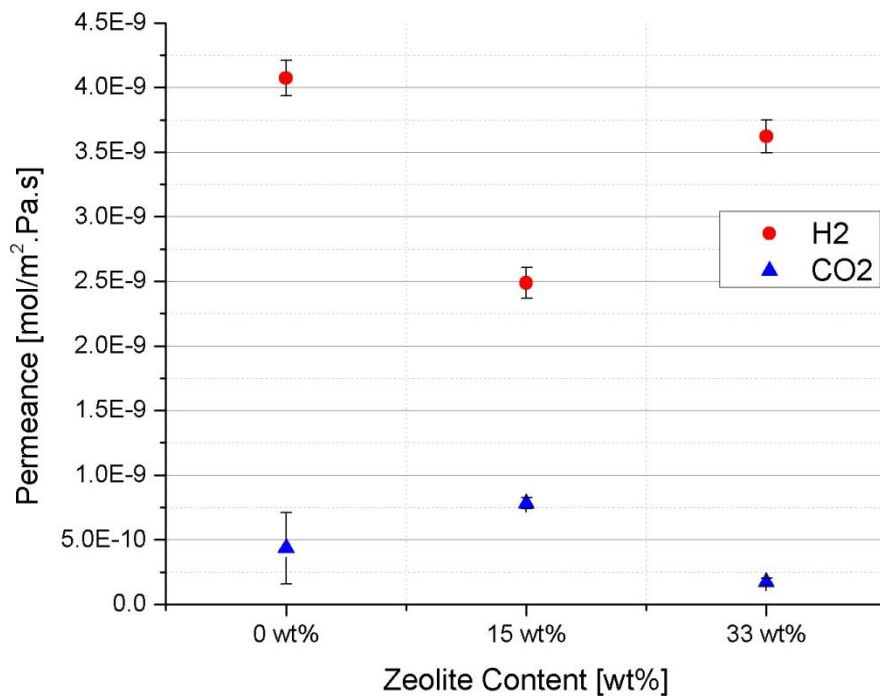
Figure 31: Permeance vs. zeolite content wt% for average values of 18 membranes at 1 bar and 25 °C

Despite the average low H_2 permeances (10^{-9} mol/m^2·Pa·s) presented in Figure 31, lower CO_2 permeances (10^{-10} mol/m^2·Pa·s) resulted in consistently reproducible H_2/CO_2 selectivities (above Knudsen) as shown in Figure 32. This means that the gas transport through the composite membranes did not flow through defects large enough to allow convective flow, but instead exhibited flow through pores with similar dimensions to the ones found in the zeolite, capable of molecular sieving. The low standard deviation of the duplicate membranes also confirms that the membrane system is not randomly selective, but instead consistently selective for all three compositions due to the reproducible microporosity screened by ALT.

Figure 32: H_2/CO_2 selectivity vs. zeolite content for 18 membranes at 1 bar and 25 °C

3.5.2 GPM Results for Varying Differential Pressure

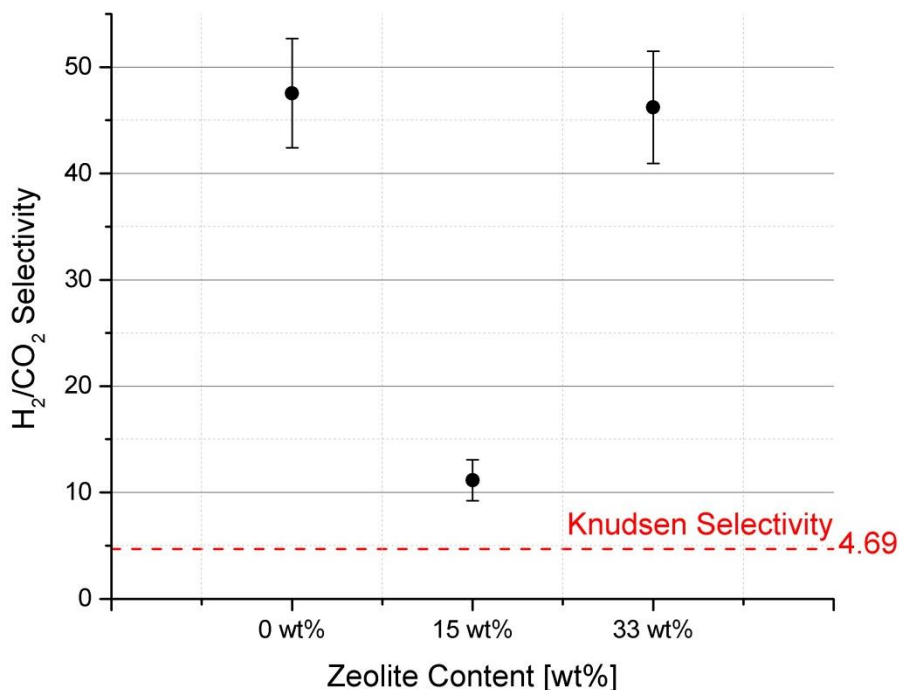Out of the 18 membrane batch, three composite membranes were selected from each of the three stable ratios (0, 15, 33 wt% zeolite) and tested under GPM with varying differential pressure.

Table 8 summarizes the ALT value for the three selected membranes (M333, M329, and M336) that met the ALT criteria for porosity. The standard deviations were below 15% and reflected the inherent variability of composition in the zeolite and cement.

Table 8: Summary of ALT for membranes M333, M329, and M336.

Membrane	Specific Air Leakage Rate [Pa·L/cm^2·s]
M333: 0 wt% zeolite	0.039 ± 10.1%
M329: 15 wt% zeolite	0.015 ± 6.1%
M336: 33 wt% zeolite	0.010 ± 10.8%

GPM was then conducted on the three membranes with increasing increments of 1 bar up to 4 bar differential pressure for H_2 and CO_2 single gases at 25 °C. The purpose of increasing pressure was to determine if the membranes remained selective beyond a 1 bar differential pressure.

3.5.2.1 GPM Results for Membrane M333 (0 wt% zeolite)

The 0 wt% zeolite (pure cement) membrane, M333, was tested first in the GPM setup. The permeance results are shown in Figure 33 while the

H_2/CO_2 selectivities are shown in Figure 34. By looking at the permeance, we can see that the CO_2 was completely rejected up to 3 bar differential pressure, while H_2 permeance increased with increasing pressure. Up to 3 bar, the CO_2 permeance was on the order of 10^{-11} mol/m^2·Pa·s which corresponds to the lowest value the flow meters can detect; the H_2/CO_2 selectivity increased from 76 to 196.
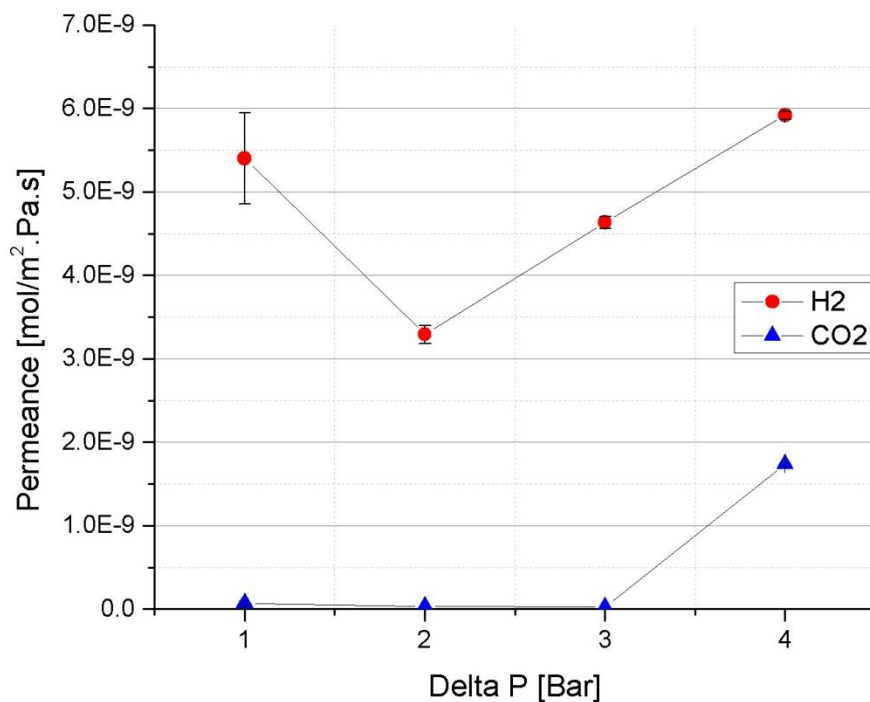
Figure 33: Permeance vs. differential pressure for membrane (M333 0 wt% zeolite) at 25 °C
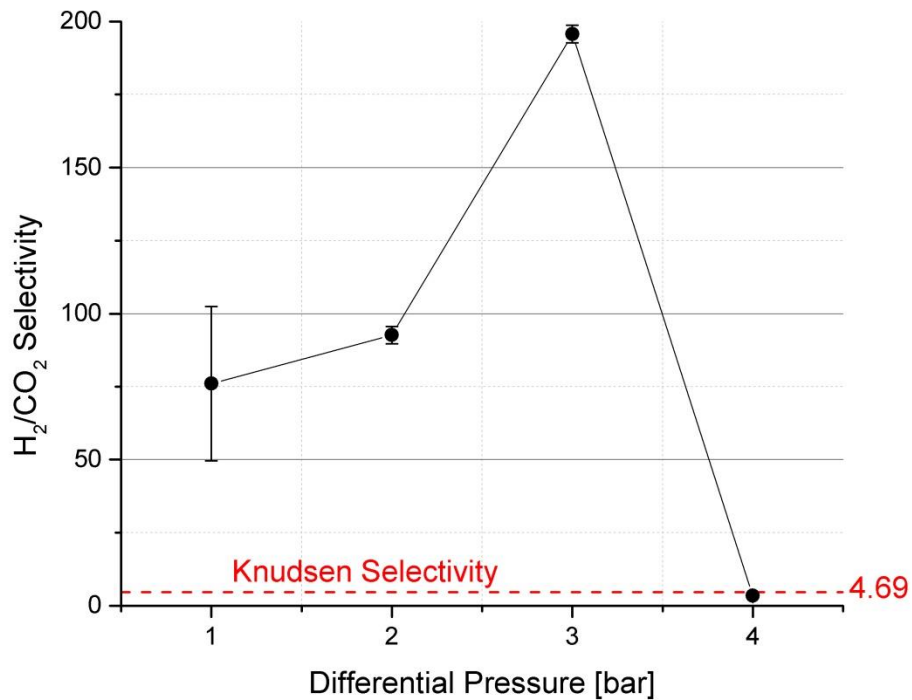
Figure 34: H_2/CO_2 selectivity vs. differential pressure for membrane M333 (0 wt% zeolite) at 25 °C

At 4 bar differential pressure, the pure cement's permeance for both H_2 and CO_2 increased significantly and the selectivity dropped to 3.4 (below Knudsen); indicating that molecular sieving was no longer occurring and the flow through defects dominated the diffusion. This can be explained by the formation of micro-cracks due to the high stress incurred on the membrane at 4 bar. When removed from the GPM setup, the membrane was visibly intact, though the test data suggests that microscopic fractures or cracks in the structure lead to the decrease in selectivity. Figure 35

shows a SEM image of the membrane's surface after testing; a small micro-crack is visible.

FZJ : IEK1 2013   EHT = 15.00 kV   Detector = SE2   WD =   8 mm   100μm
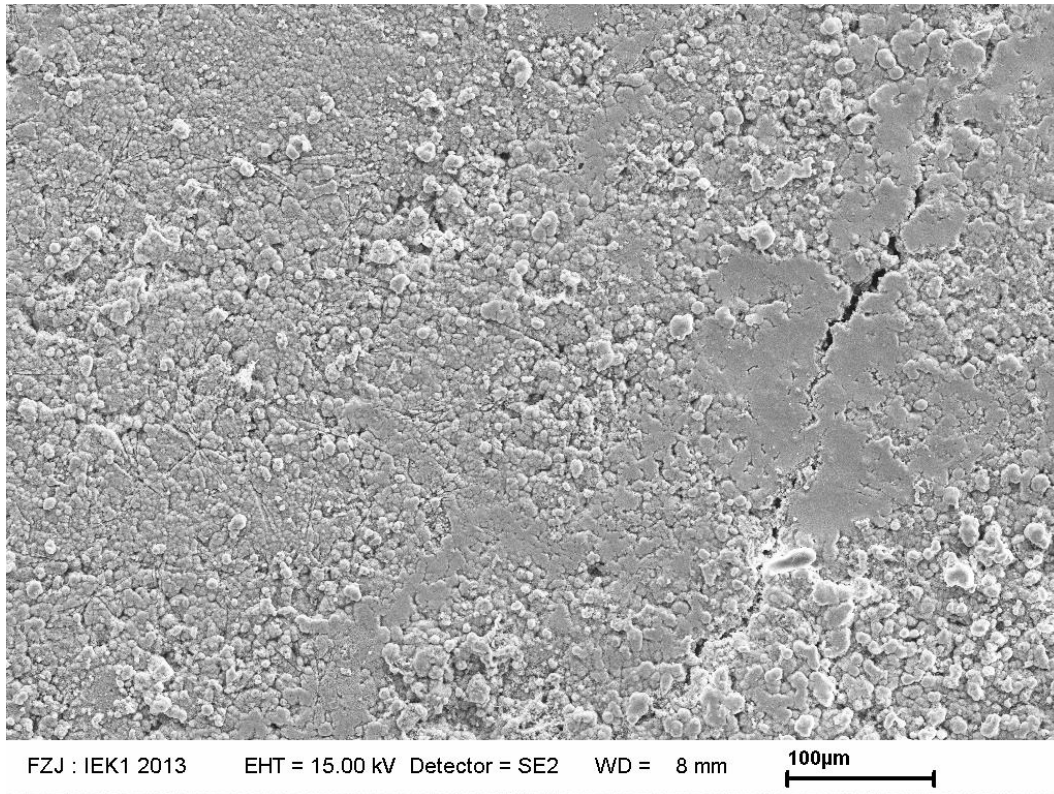
Figure 35: Surface SEM for membrane M333 (0 wt% zeolite)

As was shown in section 3.2, complete mixing had an immediate effect on the porosity of the membrane. Similarly, a small crack that is just nanometers wide can provide the path of least resistance for both gases and cause Knudsen or convective flow depending on the scale of the defect.

3.5.2.2 GPM Results for Membrane M329 (15 wt% zeolite)

The 15 wt% zeolite membrane M329's permeance and selectivity results are presented in Figure 36 and

Figure 37. Unlike the pure cement disc M333, where no significant selectivity beyond 3 bar differential pressure was displayed, M329 maintained complete CO_2 rejection up to 4 bar. The CO_2 permeance was below the detection limit of the setup on the order of 10^{-11} mol/m^2·Pa·s throughout the measurement. The H_2/CO_2 selectivities increased steadily from 29 to 115 due to increased permeance of the H_2.

Figure 36: Permeance vs. differential pressure for membrane M329 (15 wt% zeolite) at 25 °C
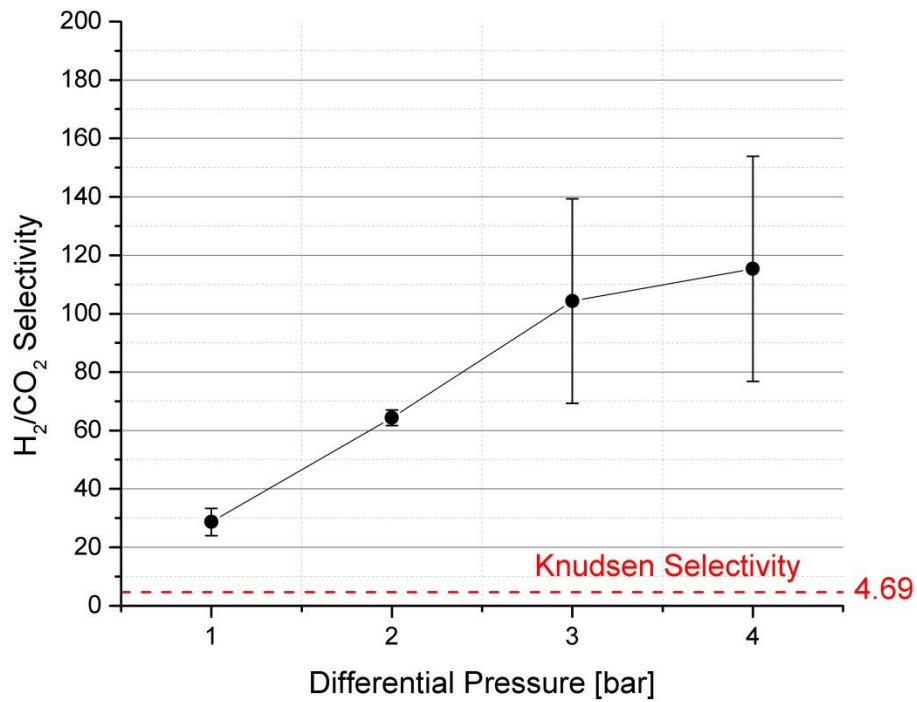
Figure 37: H_2/CO_2 selectivity vs. differential pressure for membrane M329 (15 wt% zeolite) at 25 °C

When recovered from the test system, the 15 wt% zeolite disc did not display any visible fractures. The SEM imaging of the surface showed the absence of a large micro-crack unlike the pure cement disc (Figure 38).
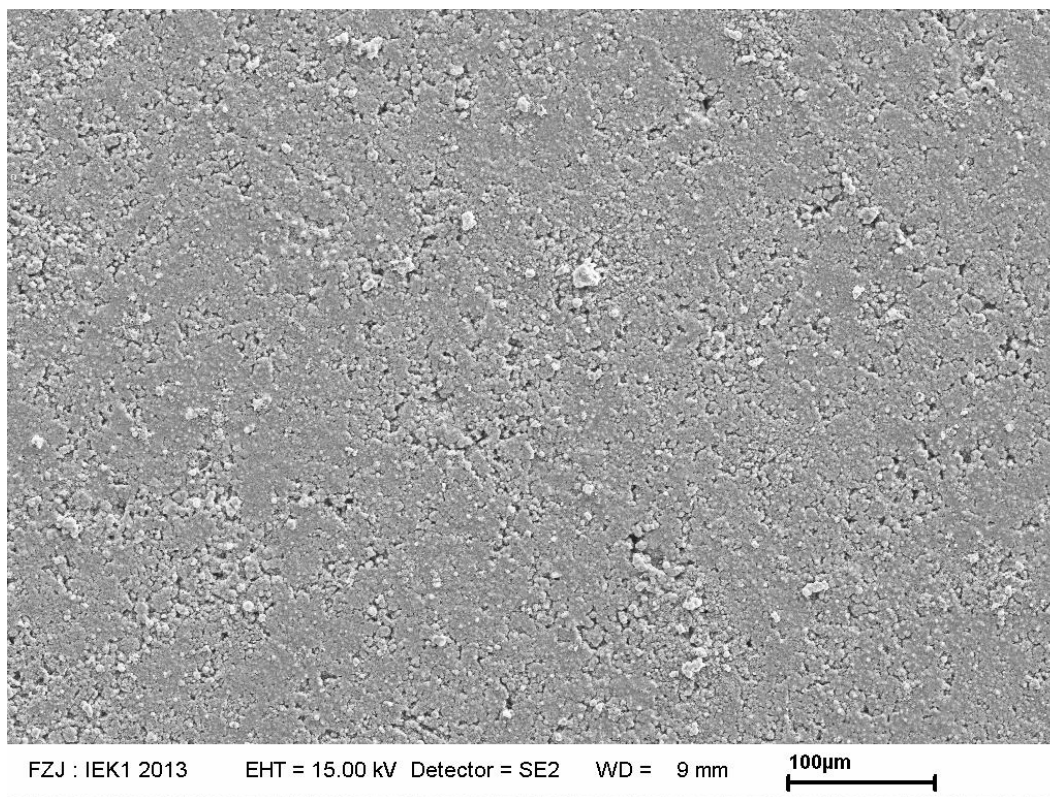
Figure 38: Surface SEM for membrane M329 (15 wt% zeolite)

3.5.2.3 GPM Results for Membrane M336 (33 wt% zeolite)

Figure 39 and Figure 40 show the GPM results for permeance and selectivity for the 33 wt% zeolite membrane, M336. It was evident that the membrane developed micro-cracks beyond 1 bar differential pressure which resulted in Knudsen flow. The CO_2 permeance increased significantly from 10^{-11} mol/m^2·Pa·s to 10^{-9} mol/m^2·Pa·s while H_2/CO_2 selectivity dropped from 77 to 3.3.
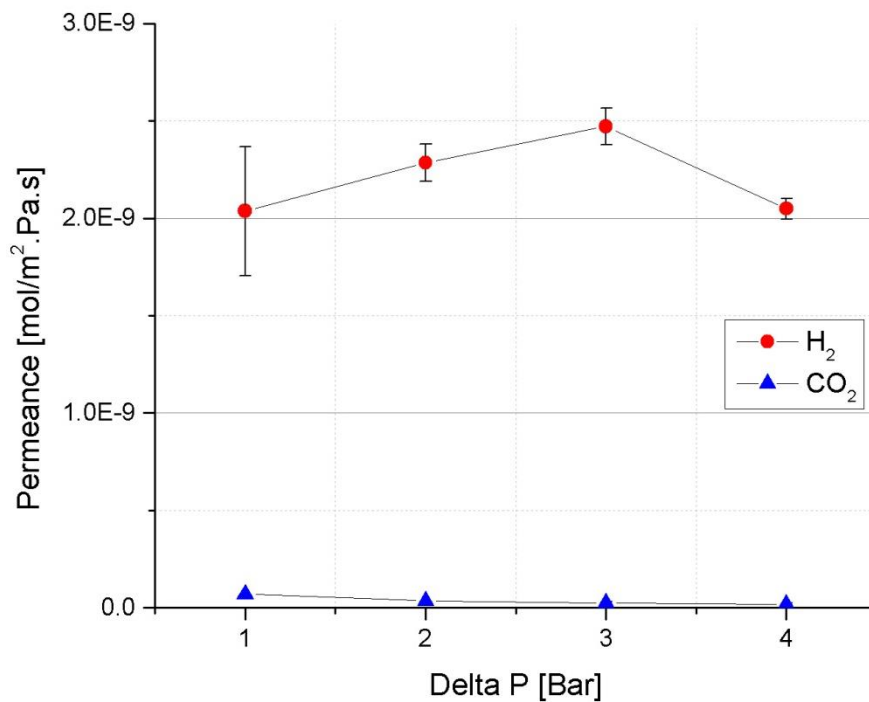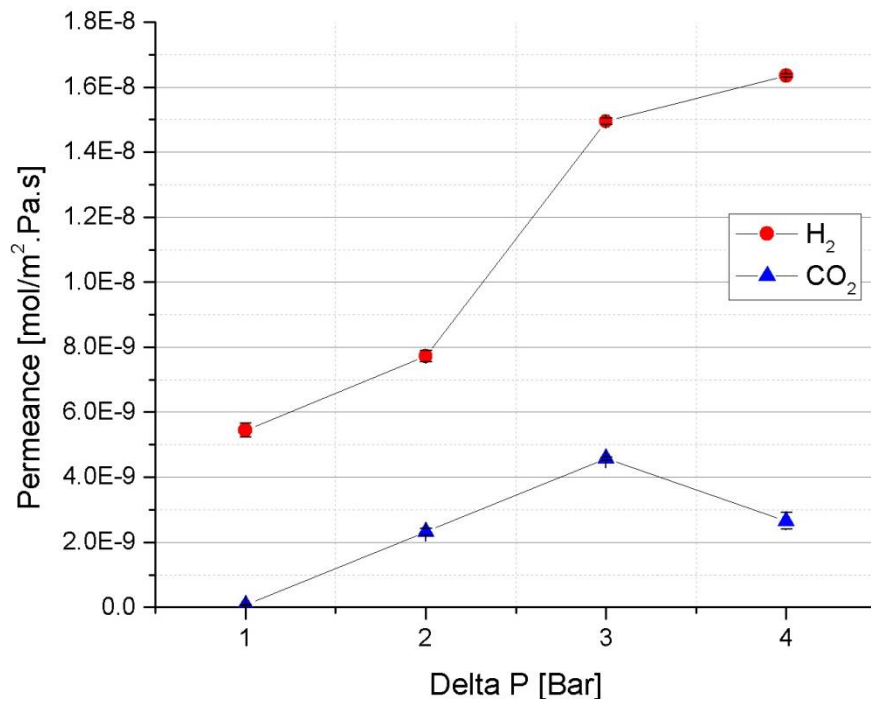
Figure 39: Permeance vs. differential pressure for membrane M336 (33 wt% zeolite) at 25 °C
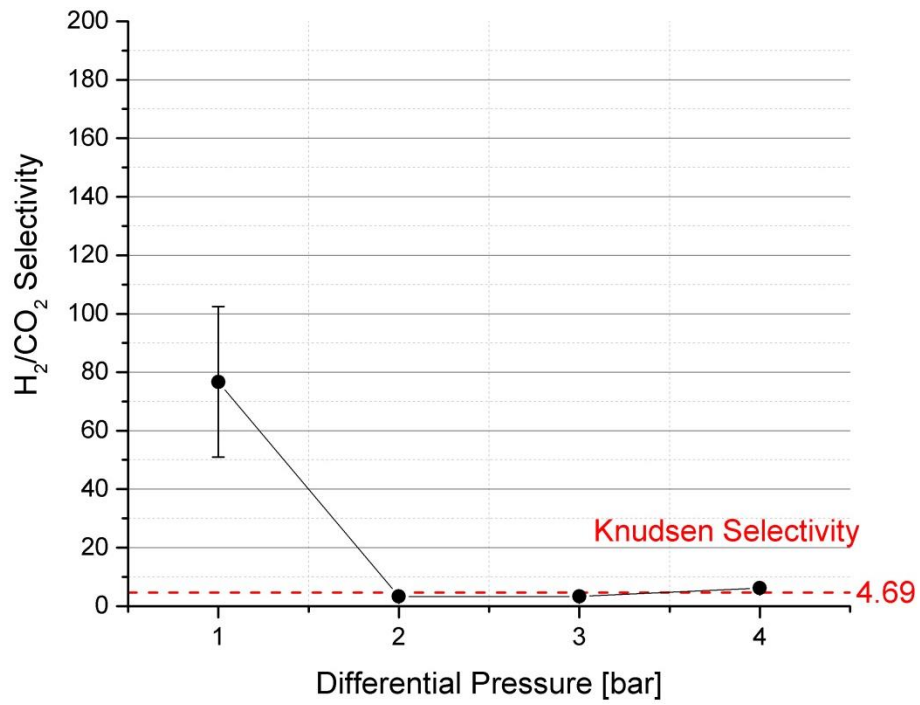
Figure 40: H_2/CO_2 Selectivity vs. differential pressure for membrane M336 (33 wt% zeolite) at 25 °C

Surprisingly, the recovered membrane did not display any fractures visually. However, under SEM imaging a defect was seen (Figure 41).
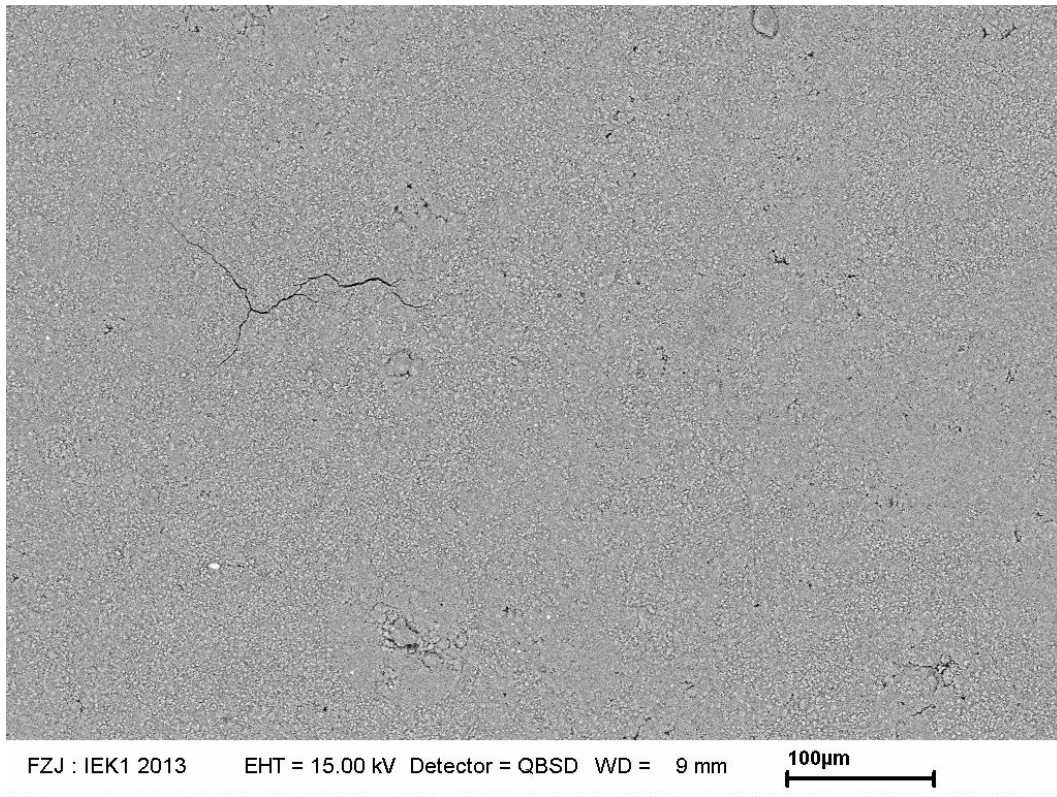
Figure 41: Surface SEM for membrane M336 (33 wt% zeolite)

Chapter 4: Conclusions and Outlook

Powder X-ray diffraction verified that the Ash Meadows clinoptilolite was at least 80% pure with high thermal stability up to 650 °C. While, particle size measurements suggested that the bimodal distribution of the cement ($D_{50}=$ 6.01 µm) would pack efficiently with the clinoptilolite powder ($D_{50}=6.97$ µm) by axial pressing.

Composite membranes were prepared for H_2 and CO_2 separation by powder pressing blended clinoptilolite/cement powders and flat bath steaming. Out of three explored steaming configurations, flat bath steaming the pressed green bodies resulted in flat mechanically stable membranes. It was also found that completely blending the clinoptilolite and cement produced membranes with desired microporosity and strength after packing.

Air leakage testing was used as a membrane pre-screening tool and allowed us to down select microporous membranes with acceptable defects suitable for permeation testing. The testing showed that the preparation method yielded high membrane reproducibility.

Membranes made of pure cement demonstrated impermeability towards CO_2, supporting the use of cement as a matrix material. Moreover, membranes having a composition beyond 33 wt% zeolite could not be tested due to significant reduction in mechanical stability.

When tested under gas permeation measurement, composite membrane ratios of 0, 15, and 33 wt% zeolite demonstrated stability up to 4 bar differential pressure and consistently met the air leakage test criteria for microporosity. Hydrogen permeances on the order of 10^{-9} mol/m$^2 \cdot$Pa$\cdot$s were obtained with low CO_2 permeances, exhibiting complete CO_2 rejection in some cases. The 10^{-9} mol/m$^2 \cdot$Pa$\cdot$s permeances obtained are comparable to typical synthetic zeolite membrane permeances of (10^{-9} to 10^{-5} mol/m$^2 \cdot$Pa$\cdot$s) [51]. The results yielded H_2/CO_2 selectivities ranging from 76-195. These selectivities were much higher than the H_2/CO_2 Knudsen selectivity of 4.69, indicating that the desired molecular sieving separation had occurred. The 15 wt% zeolite membrane showed the best performance up to 4 bar differential pressure without cracking and had a H_2/CO_2 selectivity of 115. The high H_2/CO_2 selectivity, thermal stability (within 200-500 °C syngas process requirements), scalability, and low cost, show that the prepared clinoptilolite and cement composite membranes have high potential for hydrogen production from syngas.

Additional work is necessary to further increase the zeolite content in the membranes while maintaining mechanical stability. Increasing the zeolite content would introduce higher permeances and thus higher yields. Since cement was incorporated as a matrix, the composite membrane preparation can be improved by adapting the formulations as slip coated materials on different porous supports to enhance strength. This improvement would enable an increase in permeance and offer access to

different geometries; for example, a tubular membrane would increase the surface area and thus increasing the yields.

Lifetime risks such as the reaction of carbon dioxide with cement as "carbonation" forming calcium carbonates should be investigated [54,55,56]. Further research also needs to be conducted in order determine the effect of increasing temperature on separation. While improving packing densities the powders and perhaps increasing the aggregate content to fill voids and thus defects should be studied [57].

Chapter 5: Bibliography

[1] K. Liu, C. Song and V. Subramani, Hydrogen and Syngas Production and Purification Technologies. USA: John Wiley & Sons Inc., 2009.

[2] J. W. Phair and S. P. S. Badwal, "Materials for separation membranes in hydrogen and oxygen production and future power generation," Science and Technology of Advanced Materials, vol. 7, pp. 792, 2006.

[3] H. Schlilling, B. Bonn and U. Krauss, Coal Gasification: Existing Processes and New Developments. England: Graham & Trotman Limited, 1981.

[4] C. Han and D. P. Harrison, "Simultaneous shift reaction and carbon dioxide separation for the direct production of hydrogen," Chemical Engineering Science, vol. 49, pp. 5875-5883, 1994.

[5] M. A. Nieva, M. M. Villaverde, A. Monzón, T. F. Garetto and A. J. Marchi, "Steam-methane reforming at low temperature on nickel-based catalysts," *Chem. Eng. J.,* vol. 235, pp. 158-166, 1/1, 2014.

[6] V. M. Shinde and G. Madras, "Production of syngas from steam reforming and CO removal with water gas shift reaction over nanosized $Zr0.95Ru0.05O2−δ$ solid solution," *Int J Hydrogen Energy,* vol. 38, pp. 13961-13973, 10/25, 2013.

[7] S. Adhikari and S. Fernando, "Hydrogen Membrane Separation Techniques," *Ind Eng Chem Res,* vol. 45, pp. 875-881, 02/01; 2013/11, 2006.

[8] D. W. Breck, Zeolite Molecular Sieves: Structure, Chemistry, and use. USA: Robert E. Krieger, 1984.

[9] A. Dyer, An Introduction to Zeolite Molecular Sieves. Great Britain: John Wiley & Sons Ltd., 1988.

[10] M. W. Ackley, S. U. Rege and H. Saxena, "Application of natural zeolites in the purification and separation of gases," *Microporous and Mesoporous Materials,* vol. 61, pp. 25-42, 7/18, 2003.

[11] C. S. Cundy and P. A. Cox, "The hydrothermal synthesis of zeolites: Precursors, intermediates and reaction mechanism," Microporous and Mesoporous Materials, vol. 82, pp. 1-78, 2005.

[12] (November 12, 2013). *3D frameworks obtained from the International Zeolite Association online structure database, curated from: L. B. McCusker, D. H. Olson and C. Baerlocher, "Atlas of Zeolite Framework Types," Atlas of Zeolite Framework Types, 2007.* Available: http://www.iza-structure.org/databases/.

[13] A. J. Burggraaf and L. Cot, "Fundamentals of inorganic membrane science and technology," Membrane Science and Technology, vol. 4, 1996.

[14] P. Swenson, B. Tanchuk, E. Bastida, W. An and S. M. Kuznicki, "Water desalination and de-oiling with natural zeolite membranes - Potential application for purification of SAGD process water," Desalination, vol. 286, pp. 442-446, 2012.

[15] A. S. M. Junaid, "Natural zeolite catalysts for the integrated cracking, waterless extraction and upgrading of oilsands bitumen," University of Alberta, Dissertation, 2012.

[16] A. S. M. Junaid, C. Street, W. Wang, M. M. Rahman, W. An, W. C. McCaffrey and S. M. Kuznicki, "Integrated extraction and low severity upgrading of oilsands bitumen by activated natural zeolite catalysts," Fuel, vol. 94, pp. 457-464, 2012.

[17] A. S. M. Junaid, M. Rahman, H. Yin, W. C. McCaffrey and S. M. Kuznicki, "Natural zeolites for oilsands bitumen cracking: Structure and acidity," 2011.

[18] A. Dyer, A. Chimedtsogzol, L. Campbell and C. Williams, "Uptake of caesium and strontium radioisotopes by natural zeolites from Mongolia," Microporous and Mesoporous Materials, vol. 95, pp. 172-175, 2006.

[19] A. Dyer, A. S. A. Gawad, M. Mikhail, H. Enamy and M. Afshang, "The natural zeolite, laumontite, as a potential material for the treatment of aqueous nuclear wastes," J. Radioanal. Nucl., vol. 154, pp. 265-276, 1991.

[20] A. Dyer, T. Las and M. Zubair, "The use of natural zeolites for radioactive waste treatment: Studies on leaching from zeolite/cement composites," J. Radioanal. Nucl., vol. 243, pp. 839-841, 2000.

[21] D. Papaioannou, P. D. Katsoulos, N. Panousis and H. Karatzias, "The role of natural and synthetic zeolites as feed additives on the prevention and/or the treatment of certain farm animal diseases: A review," Microporous and Mesoporous Materials, vol. 84, pp. 161-170, 2005.

[22] K. H. Nahm, "Efficient feed nutrient utilization to reduce pollutants in poultry and swine manure," Crit. Rev. Environ. Sci. Technol., vol. 32, pp. 1-16, 2002.

[23] R. W. Baker, Membrane Technology and Applications. Great Britain: John Wiley & Sons, Ltd, 2000.

[24] C. J. Geankoplis, Transport Processes and Separation Process Principles. USA: Pearson Education, Inc., 2003.

[25] "Membrane technology for liquid and gas Separations," BCC Research, Tech. Rep. MST041E, August 2010.

[26] P. Bernardo and G. Clarizia, "30 years of membrane technology for gas separation," Chemical Engineering Transactions, vol. 32, pp. 1999-2004, 2013.

[27] W. J. Koros and G. K. Fleming, "Membrane-based gas separation," J. Membr. Sci., vol. 83, pp. 1-80, 1993.

[28] R. W. Spillman and M. B. Sherwin, "Gas separation membranes: The first decade." Chemtech, vol. 20, pp. 378-384, 1990.

[29] C. J. M. van Rijn, Nano and Micro Engineered Membrane Technology. Hungary: Elsevier B.V, 2004.

[30] A. Singh and W. J. Koros, "Significance of Entropic Selectivity for Advanced Gas Separation Membranes," Industrial and Engineering Chemistry Research, vol. 35, pp. 1231-1234, 1996.

[31] W. An, P. Swenson, L. Wu, T. Waller, A. Ku and S. M. Kuznicki, "Selective separation of hydrogen from C1/C2 hydrocarbons and CO2 through dense natural zeolite membranes," J. Membr. Sci., vol. 369, pp. 414-419, 2011.

[32] T. -. Chung, L. Y. Jiang, Y. Li and S. Kulprathipanja, "Mixed matrix membranes (MMMs) comprising organic polymers with dispersed inorganic fillers for gas separation," Progress in Polymer Science (Oxford), vol. 32, pp. 483-507, 2007.

[33] S. Husain and W. J. Koros, "Mixed matrix hollow fiber membranes made with modified HSSZ-13 zeolite in polyetherimide polymer matrix for gas separation," J. Membr. Sci., vol. 288, pp. 195-207, 2007.

[34] D. C. MacLaren and M. A. White, "Cement: Its chemistry and properties," J. Chem. Educ., vol. 80, pp. 623-635, 2003.

[35] R. Snellings, G. Mertens, Ö. Cizer and J. Elsen, "Early age hydration and pozzolanic reaction in natural zeolite blended cements: Reaction kinetics and products by in situ synchrotron X-ray powder diffraction," *Cem. Concr. Res.,* vol. 40, pp. 1704-1713, 12, 2010.

[36] L. Gong, N. Jin, X. Gu and X. Jin, "Effect of curing conditions on property of high performance concrete with composite mineral admixture," Key Engineering Materials, vol. 400-402, pp. 409-414, 2009.

[37] T. Perraki, G. Kakali and F. Kontoleon, "The effect of natural zeolites on the early hydration of Portland cement," Microporous and Mesoporous Materials, vol. 61, pp. 205-212, 2003.

[38] B. Yilmaz, A. Uçar, B. Öteyaka and V. Uz, "Properties of zeolitic tuff (clinoptilolite) blended portland cement," Build. Environ., vol. 42, pp. 3808-3815, 2007.

[39] L. Alarcon-Ruiz, G. Platret, E. Massieu and A. Ehrlacher, "The use of thermal analysis in assessing the effect of temperature on a cement paste," Cem. Concr. Res., vol. 35, pp. 609-613, 2005.

[40] A. Langella, M. Pansini, G. Cerri, P. Cappelletti and M. De'Gennaro, "Thermal behavior of natural and cation-exchanged clinoptilolite from Sardinia (Italy)," Clays Clay Miner., vol. 51, pp. 625-633, 2003.

[41] (November 12, 2013). *St. Cloud Mining clinoptilolite specifications*. Available: http://www.stcloudmining.com/st-cloud-zeolite/st-cloud-data-sheets.html.

[42] B. D. Cullity, *Elements of X-Ray Diffraction.* USA: Addison-Wesley Publishing Company, Inc., 1978.

[43] M. Rhodes , *Introduction to Particle Technology.* Great Britain: John Wiley & Sons, Ltd, 2008.

[44] (November 12, 2013). *Type CEM 1 (European Standard EN 197-1).* Available:

http://www.concretecentre.com/codes__standards/eurocodes/eurocode_2/european_concrete_standards/cement,_aggregates,_admixtures.aspx.

[45] F. Podczeck and M. Sharma, "The influence of particle size and shape of components of binary powder mixtures on the maximum volume reduction due to packing," Int. J. Pharm., vol. 137, pp. 41-47, 1996.

[46] C. F. Ferraris, V. A. Hackley and A. I. Avilés, "Measurement of particle size distribution in portland cement powder: Analysis of ASTM round robin studies," Cement, Concrete and Aggregates, vol. 26, pp. 71-81, 2004.

[47] F. Saidi, Y. Bernabé and T. Reuschlé, "Uniaxial compression of synthetic, poorly consolidated granular rock with a bimodal grain-size distribution," Rock Mech Rock Eng, vol. 38, pp. 129-144, 2005.

[48] P. Vincenzini, Ceramic Powders. The Netherland: Elsevier, 1983.

[49] B. Ahmadi and M. Shekarchi, "Use of natural zeolite as a supplementary cementitious material," *Cement and Concrete Composites,* vol. 32, pp. 134-141, 2010.

[50] (November 12, 2013). *Dr. Wiesner Steuerungstechnik Integra DDV Leak Test System.* Available: http://www.drwiesner.de/en/home/products/leakage-testing-systems/integra.html.

[51] A. Julbe, "Chapter 6 Zeolite membranes - synthesis, characterization and application," Studies in Surface Science and Catalysis, vol. 168, pp. 181-219, 2007.

[52] A. Chougnet-Sirapian, E. Pershikova and A. Loiseau, "New steam resilient cement: Evaluation of long-term properties under extreme conditions," in Proceedings - SPE International Symposium on Oilfield Chemistry, 2011, pp. 440-454.

[53] Z. He, Y. Xie, B. Liu and G. Long, "High performance steam-cured concrete for railway precast elements," in Proceedings of the 2nd International Conference on Transportation Engineering, ICTE 2009, 2009, pp. 2084-2089.

[54] B. Huet, V. Tasoti and I. Khalfallah, "A review of portland cement carbonation mechanisms in CO 2 rich environment," in Energy Procedia, 2011, pp. 5275-5282.

[55] S. Monkman and Y. Shao, "Carbonation curing of slag-cement concrete for binding CO2 and improving performance," J. Mater. Civ. Eng., vol. 22, pp. 296-304, 2010.

[56] S. Rukzon and P. Chindaprasirt, "An experimental investigation of the carbonation of blended portland cement palm oil fuel ash mortar in an indoor environment," Indoor and Built Environment, vol. 18, pp. 313-318, 2009.

[57] A. K. H. Kwan and H. H. C. Wong, "Packing density of cementitious materials: Part 2-packing and flow of OPC + PFA + CSF," Materials and Structures/Materiaux Et Constructions, vol. 41, pp. 773-784, 2008.